

#### Contents lists available at ScienceDirect

#### Cancer Letters

journal homepage: www.elsevier.com/locate/canlet



#### Original Articles

# *HOTAIRM1* lncRNA is downregulated in clear cell renal cell carcinoma and inhibits the hypoxia pathway



Michael J. Hamilton<sup>a</sup>, Matthew Young<sup>a</sup>, Kay Jang<sup>a</sup>, Silvia Sauer<sup>a</sup>, Vanessa E. Neang<sup>a</sup>, Alexia T. King<sup>a</sup>, Thomas Girke<sup>b</sup>, Ernest Martinez<sup>a,\*</sup>

- <sup>a</sup> Department of Biochemistry, University of California, Riverside, CA, USA
- b Department of Botany and Plant Sciences, University of California, Riverside, CA, USA

#### ARTICLE INFO

# Keywords: Long non-coding RNA ccRCC Kidney lineage Cell differentiation Hypoxia-Inducible Factor 1α (HIF1α)

#### ABSTRACT

HOXA Transcript Antisense RNA, Myeloid-Specific 1 (HOTAIRM1) is a conserved long non-coding RNA (lncRNA) involved in myeloid and neural differentiation that is deregulated in acute myeloid leukemia and other cancers. Previous studies focused on the nuclear unspliced HOTAIRM1 transcript, however cytoplasmic splice variants exist whose roles have remained unknown. Here, we report novel functions of HOTAIRM1 in the kidney. HOTAIRM1 transcripts are induced during renal lineage differentiation of embryonic stem cells and required for expression of specific renal differentiation genes. We show that the major HOTAIRM1 transcript in differentiated cells is the spliced cytoplasmic HM1-3 isoform and that HM1-3 is downregulated in > 90% of clear cell renal cell carcinomas (ccRCCs). Knockdown of HM1-3 in renal cells deregulates hypoxia-responsive and angiogenic genes, including ANGPTL4. Furthermore, HOTAIRM1 transcripts are downregulated by hypoxia-mimetic stress and knockdown of the cytoplasmic HM1-3 isoform in normoxic cells post-transcriptionally induces Hypoxia-Inducible Factor  $1\alpha$  ( $HIF1\alpha$ ) protein, a key activator of ANGPTL4. Our results demonstrate the pervasive downregulation of the specific HOTAIRM1 cytoplasmic isoform HM1-3 in ccRCC and suggest possible roles of HOTAIRM1 in kidney differentiation and suppression of HIF1-dependent angiogenic pathways.

#### 1. Introduction

Kidney and renal pelvis cancers are among the most pervasive cancers found within the United States [1]. Renal cell carcinomas (RCCs) comprise > 90% of kidney cancers, which have been shown to be particularly difficult to treat with conventional therapies [2-4]. Among these, the clear cell renal cell carcinoma (ccRCC) type accounts for 75% of all kidney cancers [5]. The Von Hippel-Lindau (VHL) tumor suppressor gene is the most frequently mutated gene in sporadic ccRCC and codes for the substrate recognition subunit of an E3 ubiquitin ligase complex that targets the Hypoxia-Inducible Factors  $1\alpha$  and  $2\alpha$  (HIF1  $\alpha$ and HIF2 α) for proteasomal degradation [6]. Hence, the VHL-HIF axis is often altered in ccRCC tumors, which are highly vascularized due to hyperactivation of various HIF target genes involved in angiogenesis. Recently, additional genetic alterations have been associated with ccRCC development [7], and transcriptomic analyses have identified several long non-coding RNAs (lncRNAs) that are deregulated in ccRCC [8,9]. One notable example is the lncRNA PVT1, which increases the stability of the MYC oncoprotein [10], while the PVT1 promoter locus was shown to inhibit MYC transcription [11]. PVT1 is part of a network of lncRNAs that modulates MYC activity and consequently the VHL-HIF axis by affecting the binding partners of HIF1 $\alpha$  and HIF2 $\alpha$  in ccRCC [12–15].

However, only few lncRNAs have been extensively explored in RCC/ ccRCC [16]. In our recent bioinformatics studies examining isoformspecific transcript alterations in ccRCC tumors, we identified several candidate deregulated lncRNAs, potentially including HOTAIRM1 [17]. The HOTAIRM1 locus is located within the HOXA cluster between (and antisense to) the HOXA1 and HOXA2 genes. HOTAIRM1 is best known for its role in activation of the HOXA genes during neural differentiation of pluripotent cells and differentiation of promyelocytic leukemia cells via binding MLL and PRC2 and altering chromatin structure in cis at the HOXA locus [18-20]. However, contrary to its original designated name, HOTAIRM1 expression has now been reported in numerous developing and fully differentiated tissues and cell types, and HOTAIRM1 expression is altered in several human cancers [21-24]. While the mechanistic roles of HOTAIRM1 in cancer are largely unknown, recent evidence in NB4 promyelocytic leukemia cells suggests a function in the autophagy pathway via acting as a miRNA sponge [25].

In the current study, we report for the first time a role of *HOTAIRM1* 

<sup>\*</sup> Corresponding author. Department of Biochemistry, University of California Riverside, 900 University Avenue, Riverside CA 92521, USA. *E-mail address*: ernest.martinez@ucr.edu (E. Martinez).

during renal lineage differentiation and the pervasive downregulation of specifically its spliced isoform HM1-3 in >90% of ccRCC tumors cataloged in the Cancer Genome Atlas (TCGA) database. Using a model kidney proximal tubule ccRCC cell line (CAKI-1) that is VHL-positive and expresses all HOTAIRM1 isoforms, we demonstrate that the cytoplasmic isoform HM1-3 suppresses HIF1 $\alpha$  protein levels and attenuates hypoxia-responsive target genes under normoxic conditions. Our results suggest possible pro-differentiation and tumor-suppressive roles of HM1-3 in the kidney via inhibition of the oncogenic HIF1 pathway, which is activated in the vast majority of ccRCC tumors.

#### 2. Materials and methods

#### 2.1. Cell culture

The HK-2, ACHN and CAKI-1 cell lines were acquired from ATCC and were cultured as recommended. The HK-2 cell line was cultured in keratinocyte serum-free medium supplied with 0.05 mg/ml bovine pituitary extract and 5 ng/ml human recombinant epidermal growth factor (Invitrogen, Carlsbad, CA), unless otherwise indicated. The ACHN cell line was cultured in Dulbecco's modified Eagle's medium supplemented with 10% FBS (Gibco, Grand Island, USA). The CAKI-1 cell line was cultured in McCoy's 5a Modified Medium supplemented with 10% FBS (Gibco, Grand Island, USA), unless otherwise indicated. All cultures were maintained in a humidified incubator with 5% CO<sub>2</sub> at 37 °C. Mouse embryonic stem (mES) cell line D3 (CRL-11632) and mES KH2 cell line (MESKH2 B912) were purchased from ATCC and Mirimus, respectively, and cultured in pluripotency media according to manufacturers' specifications. Generation of KH2 mouse ES cell lines with doxycycline-inducible shRNAs was as previously described [26] (see Supplemental Information). The mES cells were grown and expanded on a monolayer of Mitomycin C treated primary mouse embryo fibroblasts (MEFs). Before each experiment, MEFs were removed and mES cells were expanded on 0.1% gelatin-coated cell culture dishes. Pluripotency media contained DMEM with high glucose, 15% FBS, 2 mM Lglutamine, 0.1 mM non-essential amino acids, 0.1 U/ml penicillin,  $0.1 \,\mu g/ml$  streptomycin,  $0.55 \,mM$  2-mercaptoethanol and  $1000 \,U/ml$  of Leukemia Inhibitory Factor (LIF). For KH2 cells the medium was further complemented with 2i (1  $\mu$ M PDO325901 + 2  $\mu$ M CHIR99621) per manufacturer's instructions. For retinoic acid (RA)-induced differentiation towards early neural lineage, mES cells were cultured in medium without LIF or 2i and supplemented with  $10^{-6}\ M$  all-trans retinoic acid (R625, Sigma), and medium was changed every 24 h for the indicated times. For early renal lineage differentiation KH2 mES cells were differentiated as previously described (Nishikawa et al., 2012). Briefly, cells were seeded at a density of  $6.4 \times 10^2$  cells/cm<sup>2</sup> in medium (as above without LIF or 2i) and supplemented sequentially with differentiating factors: 10 ng/ml Activin A, 50 ng/ml BMP-4, 10 mM LiCl, and 100 nM RA. Each factor was added in succession in the above order and cumulatively, starting at the time of plating and every 48 h thereafter. Cells were collected by trypsinization after 8 days for RNA extraction and quantitative PCR analysis.

#### 2.2. RNA extraction and reverse transcription-quantitative PCR (RT-qPCR)

Cells were collected using 0.25% trypsin and total RNA was extracted using the GeneJet RNA purification kit (Thermoscientific, Carlsbad, CA) per manufacturer's recommendations. DNA was digested using the RNase-Free DNase set (Qiagen, Valencia, CA) for 1 h on the column according to the manufacturer's instructions. Total RNA from mouse ES cells was purified using the Direct-Zol RNA kit (Zymo Research). Extracted RNA was verified for quality and quantity using gel electrophoresis and the Thermoscientific Nanodrop2000 spectrophotometer. cDNA was synthesized using 1 µg of total RNA using the iScript reverse transcription supermix (Biorad, Irvine, CA) according to the manufacturer's instructions. Quantitative PCR (qPCR) was

performed using the Biorad iQ SYBR green supermix and a Biorad CFX Connect thermocylcer (Biorad, Irvine, CA) and analyzed using the CFX manager software. Using a single threshold Cq determination, the Livak method was employed for all gene expression analyses. Expression analyses in renal cells and tissues were normalized to PPIA, as PPIA was found to be the most suitable reference gene when comparing ccRCC tumors to normal adjacent tissue [27,28], and no significant change was observed with HOTAIRM1 knockdown. The 12 ccRCC tumor/ normal matched pair RNA samples were obtained from Origene (see Supplemental Information). The multiple human tissue cDNA arrays were obtained from Origene (CSRT301, HKRT102) and were normalized to ACTB. Expression analyses in mouse ES cells were normalized to three housekeeping genes (Gapdh, Rpol2, and Actb). Three technical replicates of each biological replicate were performed for every qPCR reaction using the aforementioned protocols, reagents and instrumentation.

#### 2.3. Primer design

Primers sequences were obtained either from qPrimerDepot (https://primerdepot.nci.nih.gov/) or designed using Primer3Plus (www.primer3plus.com/) using the qPCR settings and adhered to the specifications set forth by the manufacturer of the qPCR equipment used (Bio-Rad), including primer efficiencies. (see Supplemental Information). All primers were synthesized by Integrated DNA Technologies.

#### 2.4. Nuclear and cytoplasmic RNA expression analysis

Approximately 1 million cells were lysed in 175  $\mu$ l of cytoplasmic lysis buffer (50 mM TrisCl pH 8.0, 140 mM NaCl, 1.5 mM MgCl2, 0.5% P-40, 1 mM DTT) on ice for 5 min for the HK-2 and CAKI-1 cells and 35 min for the ACHN cells. Following incubation, the lysate was spun at 300 g for 2 min at 4 °C. Cytoplasmic supernatant and nuclear pellet were separated, and RNA was purified as above. Corresponding cell equivalents of cytoplasmic and nuclear RNA were used for reverse transcription and qPCR.

#### 2.5. siRNA transfection and RNA-seq analyses

All custom siRNAs (Supplemental Information) were designed using the MIT Whitehead software (http://sirna.wi.mit.edu/) and synthesized as "Silencer Select siRNAs" by Ambion (Carlsbad, CA, USA). The validated Silencer Select negative siRNA #2 (Ambion) was used as control in transient knockdown assays. siRNAs were transfected using Lipofectamine3000 per manufacturer's recommendations at a final concentration of 100 nM. Total cellular RNA was extracted 60 h after transfection. For knockdown of mouse Hotairm1 in differentiated renal cell progenitors, a Silencer Select siRNA "e3-3.7" (Supplemental information) which targets exon 3 of mouse Hotairm1 was transfected with Lipofectamine 3000 per manufacturer's recommendations at a concentrations of 10 nM in differentiation medium.

For RNA-seq analysis, three biological replicates of siRNA-transfected CAKI-1 cells were trypsinized and total RNA was extracted, as above. RNA quality and quantity were evaluated with a bioanalyzer and Thermoscientific Nanodrop2000 spectrophotometer. Single-end read RNA-seq libraries were constructed using the NEBNext Ultra Directional RNA library prep kit (Illumina). Samples were multiplexed and sequenced with the NEX-seq Illumina sequencing platform at the UCR Core Genomics Facility. The RNA-seq data can be accessed at NCBI's Gene Expression Omnibus (GEO) under number GSE136604.

#### 2.6. Bioinformatic analyses

A total of 542 fastq RNA-seq files were downloaded from The Cancer Genome Atlas (TCGA) legacy archive website (https://portal.

gdc.cancer.gov/legacy-archive/search/f). Human cDNA and ncRNA FASTA formatted transcript files (Ensembl v89 annotation) were acquired form the Ensembl ftp site (https://www.ensembl.org/info/data/ftp/index.html), and merged to create a master file of all putative coding and non-coding transcripts.

Transcript quantifications and differential expression analyses were performed using the cufflink suite (TCGA data analysis) or the kallistosleuth pipeline (RNA-seq analysis) [29–31]. Cufflinks was used to obtain transcript quantifications [30]. Calculated transcript quantifications were then used to generate tumor/normal ratios. A two-tailed Wilcoxon signed rank test was performed to determine statistical significance. Cuffdiff was used to confirm differential expression. Using the default settings, kallisto was used to create an index for quantification using the aforementioned FASTA master file. Subsequently, kallisto was used to quantify all putative transcripts using 50 bootstrap samples. Differential expression analysis was performed with sleuth using the Wald test with a cutoff of q-value < 0.05 and beta > 0.5.

For the gene-level analyses, alignment of the fastq files was performed first with HISAT2 using the hg38 human assembly [32]. Read counting was performed using the summarizeOverlaps package, with union mode [33]. Using the read counts, an edgeR analysis was performed using the default settings [34,35]. The entire pipeline was performed within the systemPipeR package [32,36]. Normalization of the gene counts was performed using DESeq2 and then subsequently used in consensus clustering to determine the number molecular subtypes in ccRCC [37]. Consensus clustering was performed using the ConsensusClusterPlus R package [38]. A total 1,000 of the most variable genes, based on mean absolute deviation were used in the clustering generating consensus matrices for k = 2–7. Number of molecular subtypes was determined based on the consensus matrices and the cumulative distribution functions for each k.

#### 2.7. Western blot

Cells were scraped and lysed using RIPA buffer (150 mM NaCl, 5 mM EDTA, 50 mM Tris pH 8.0, 1% NP-40, 0.5% sodium deoxycholate, 0.1% SDS). Lysate was spun in a microfuge at maximum speed and the soluble protein concentration was determined using Bradford reagent (Biorad). A total of 10–20  $\mu$ g protein was subjected to SDS-PAGE. Proteins were transferred to a nitrocellulose membrane using a Trans-Blot Turbo (Biorad) for 45 min at 25 V. Membranes were blocked with 1% non-fat dry milk for 1 h and probed overnight with primary antibodies,  $\beta$ -actin at 1:7500 (sc-47778, Santa Cruz Biotech.), DDAH1 at 1:1000 (sc-514841, Santa Cruz Biotech.), VHL at 1:3000 (sc-17780, Santa Cruz Biotech.), and HIF1 $\alpha$  at 1:3000 (ab179483, Abcam). Secondary HRP-conjugated antibodies, anti-mouse and anti-rabbit, were incubated at 1:1000 dilution for 1 h at room temperature and chemiluminescence reactions were performed as per manufacturer's instructions (GE Healthcare).

#### 3. Results

#### 3.1. The HOTAIRM1 spliced isoform HM1-3 is downregulated in ccRCC

We initially performed a survey of *HOTAIRM1* transcripts in 8 different cancers and cognate normal tissues by qPCR using a multiple tissue cDNA array (Fig. 1A and B, Supplemental Fig. 1A and B). This revealed a significant downregulation of the spliced *HM1-3* isoform in kidney cancer, renal cell carcinomas (RCCs). *HM1-3* downregulation was also observed in breast and colorectal cancers, consistent with previous reports [21,39]. Examination of *HM1-3* expression specifically in clear cell RCC (ccRCC) and in papillary RCC (pRCC), using an independent cDNA array, demonstrated that *HM1-3* downregulation was significant in ccRCC (Fig. 1C). An average ~5.5 fold downregulation in *HM1-3* expression was seen when comparing 9 normal renal tissue samples to 21 ccRCC samples. No statistically significant *HM1-3* 

downregulation was observed in the 10 pRCC tumors tested. These results were supported further using 12 ccRCC matched pair samples, which showed 11 ccRCC tumors with a *HM1-3* downregulation relative to their normal adjacent tissue (Fig. 1D). In contrast, there were no statistically significant differences in expression of the *HM1-2-3* isoform or the *unspliced HOTAIRM1* transcript (Fig. 1D).

To further substantiate HM1-3 downregulation in ccRCC, 614 RNAseq datasets (72 normal and 542 ccRCC samples) from TCGA were bioinformatically examined. Evaluation of HOTAIRM1 FPKM tumor/ normal ratios, using 50 matched pair samples contained within these datasets, confirmed the above qPCR results showing that HM1-3 is the only significantly downregulated HOTAIRM1 transcript, as determined by Wilcoxon signed ranked test (Fig. 1E). Notably, 46 of the 50 tumors (92%) had greater than 2-fold reduction in HM1-3 levels compared to their normal adjacent tissue. Data from the GTEx database (https:// gtexportal.org/home/) confirmed that HOTAIRM1 is significantly expressed in normal kidney cortex relative to other tissues (Supplemental Fig. 2A). We further examined the expression levels of the different HOTAIRM1 transcripts by merging the RNA-seq alignments files from the 72 normal adjacent renal tissues of TCGA, which indicated that inclusion of exon 2 is rare (Fig. 1F, top), and by quantifying the different transcripts using cufflinks (Supplemental Fig. 2B). This showed that the HM1-3 isoform is the most abundant HOTAIRM1 transcript in normal renal tissue. The predominance of HM1-3 over the HM1-2-3isoform was further supported by endpoint PCR using 12 normal renal tissue samples (Fig. 1F, bottom).

As ccRCC is a herterogeneous cancer, HM1-3 expression was explored within the different molecular subtypes of ccRCC. Consensus clustering was performed using gene-level read counts from the 542 ccRCC samples, which confirmed the existence of four molecularly distinct subtypes of ccRCC (Fig. 1G, left, clusters 1-4; Supplemental Fig. 3) corresponding to the previously reported ccA, ccB, mixed ccA/ ccB and distal tubule subtypes [7,9]. Using a two-tailed Student's t-test, a significant HM1-3 downregulation was found within all four subtypes of ccRCC (Fig. 1G, right; p < 0.05). Our attempts to stratify HM1-3 expression levels according to ccRCC tumor stage or grade in the TCGA datasets did not retrieve a significant correlation, nor did we find a correlation with patient survival, suggesting that HM1-3 downregulation might be an early event in ccRCC development (data not shown). Altogether, these results identify the spliced HM1-3 isoform as the major HOTAIRM1 transcript in non-tumor renal tissue and indicate its widespread downregulation in ccRCC tumors of all subtypes, including in over 90% of ccRCC tumors for which matched normal adjacent tissue data were available in TCGA.

3.2. Expression of HOTAIRM1 spliced isoforms is associated with the non-transformed and differentiated phenotypes of renal and non-renal cell types

Several human renal proximal tubule epithelial cell lines were investigated for their HOTAIRM1 expression by RT-qPCR, including normal immortalized cells (HK-2) and two ccRCC cell lines (ACHN and CAKI-1). Absolute levels of the spliced transcripts were very low in all cell lines tested. The highest amounts of the spliced HM1-3 and HM1-2-3 transcripts were observed in CAKI-1 cells, which contained approximately 10 copies each per cell (Fig. 2A). All the immortalized and cancer cell lines tested expressed lower levels of the spliced isoforms relative to the unspliced HOTAIRM1 transcript (Fig. 2A), reminiscent of the preferential downregulation of the HM1-3 isoform in ccRCC tumors (see above and Supplemental Fig. 4). Other non-renal immortalized or cancer cell lines of the breast (MCF10A and MCF7), and brain (DAOY) showed comparable or lower levels of the spliced isoforms and a predominance of the unspliced HOTAIRM1 transcript (data not shown). Subcellular fractionation showed that the spliced isoforms HM1-3 and HM1-2-3 are predominantly cytoplasmic, while the unspliced HO-TAIRM1 transcript is mostly nuclear (Fig. 2B).

Given the reduced expression of the spliced HM1-3 isoform in

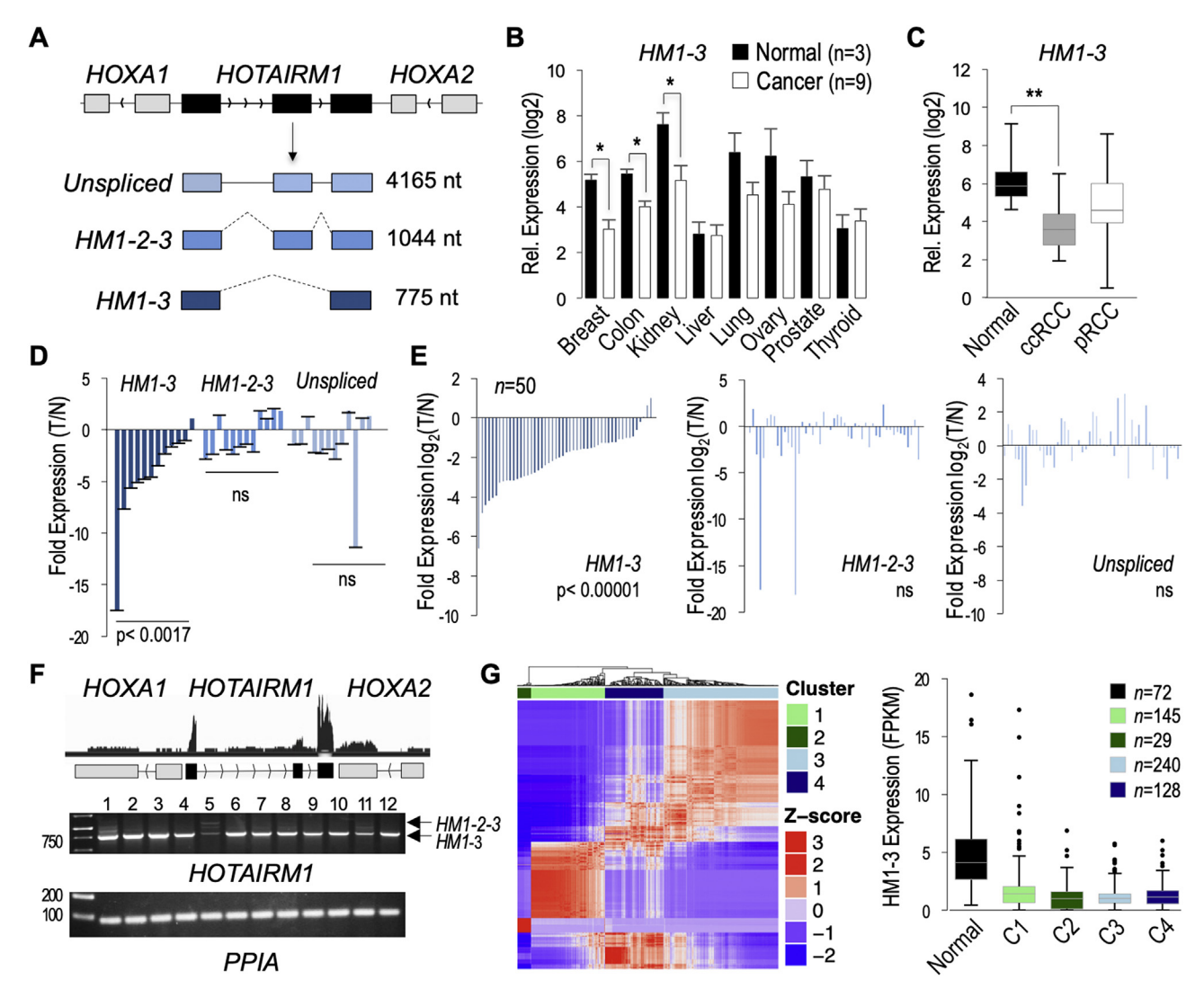
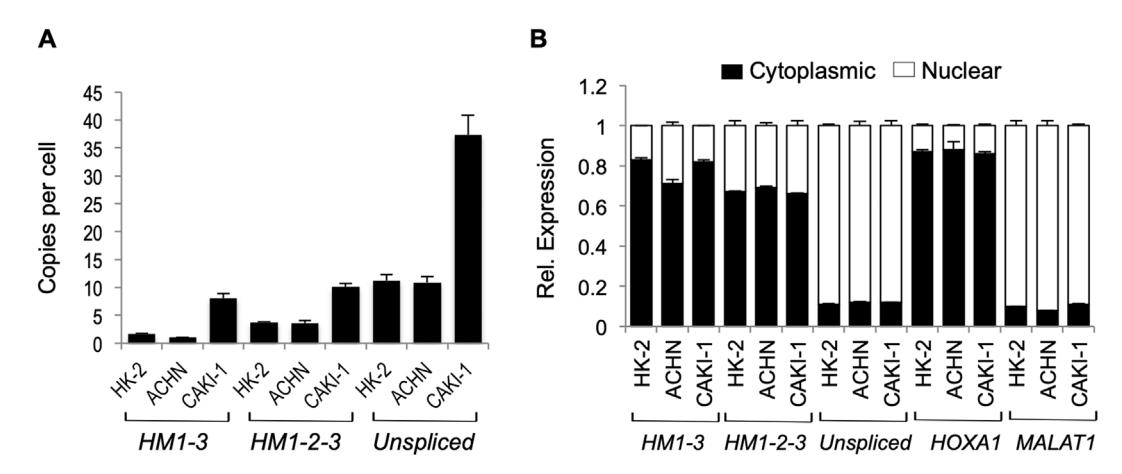


Fig. 1. Reduced HM1-3 expression in ccRCC. A. The HOTAIRM1 gene is located between HOXA1 and HOXA2 and produces an unspliced transcript and two major spliced RefSeq transcripts (HM1-3, HM1-2-3). B. Relative qPCR expression analysis of HM1-3 in a panel of eight human cancers (n = 9 tumors each) and their respective normal tissues (n = 3 each). HM1-3 levels were normalized to β-actin. C. Analysis of HM1-3 expression by qPCR in normal tissues (n = 9) versus ccRCC (n = 21) and pRCC (n = 10, papillary renal cell carcinoma) tumors was performed as in panel B. D. Analysis of HM1-3 expression by qPCR in 12 ccRCC matched pair samples. Fold changes in expression in tumor vs normal (T/N) ( $\Delta\Delta$ Ct) are indicated. E. FPKM tumor/normal ratios of 50 ccRCC matched pair TCGA samples for all HOTAIRM1 transcripts. F. Quantification of HOTAIRM1 transcripts within normal adjacent tissues. Shown is the merged trace of 72 normal renal RNA-seq datasets of TCGA (top) and a validation using 12 independent normal renal RNA samples using endpoint RT-PCR with primers in exon 1 and 3 (bottom); PCR products for HM1-3 and HM1-2-3 are indicated with arrows. G. Unsupervised consensus clustering identified 4 distinct ccRCC subtypes (left). HM1-3 expression (FPKM) is decreased in each ccRCC tumor subtype (right). Statistical significance was determined by using two-tailed Student's t-test for panels B, C, and G and the Wilcoxon signed rank test for the matched pair samples in panels D and E (\*p < 0.05, \*\*p < 0.005, ns p > 0.01).

immortalized/cancer cell lines and in ccRCC tumors compared to normal renal tissue, we further analyzed HM1-3 expression during normal cell differentiation. Since HOTAIRM1 was shown to be induced during neural differentiation of pluripotent embryonal carcinoma NT2/ D1 cells [20], we first characterized the different Hotairm1 isoforms and their expression during retinoic acid (RA)-induced early neural lineage differentiation of normal mouse ES cells in vitro. All Hotairm1 transcripts were rapidly induced and the mouse HM1-3 paralog (E1-3) was by far the most abundant isoform (average ~50 copies/cell after 3 days) and accumulated in the cytoplasm with kinetics similar to the induction of the Hoxa1 mRNA (~30 copies/cell after 3 days) (Supplemental Fig. 5 and data not shown). Similar results were obtained during differentiation of mouse ES cells into early renal lineage progenitor cells (see further below). Altogether these results indicate that the spliced HM1-3 isoform is highly induced during normal cell differentiation (both neural and renal differentiation) but its expression is suppressed in immortalized/cancer cell lines in vitro and in ccRCC tumors in vivo.

# 3.3. HOTAIRM1 regulates genes involved in the hypoxia pathway and in early renal lineage differentiation

To investigate the functions of *HOTAIRM1* we performed knockdown experiments in CAKI-1 cells, as this cell line had the highest levels of *HOTAIRM1* transcripts among all the renal proximal tubule epithelial cell lines analyzed (see above). Of the three siRNAs tested, siRNA #1 did not efficiently reduce expression of *HOTAIRM1*, while siRNAs #2 and #3 were effective in knocking down both spliced isoforms but did not affect the levels of the nuclear unspliced *HOTAIRM1* transcript under the conditions used (Fig. 3A). This provided us with conditions to selectively test the functions of the spliced isoforms. We hypothesized that albeit cytoplasmic the spliced isoforms could nevertheless influence gene expression and the levels of specific mRNAs. To test this, we performed a stranded RNA-seq analysis of cells transfected with



**Fig. 2.** Characterization of *HOTAIRM1* transcripts in renal proximal tubule cell lines. A. Copies per cell using qPCR. Error bars represent SEM across three biological replicates. **B.** Subcellular localization of transcripts. As controls the nuclear *MALAT1* lncRNA and cytoplasmic *HOXA1* mRNA were analyzed. Error bars represent SEM for three replicates.

negative control siRNA or specific siRNA #2 (Fig. 3B). Combining edgeR and kallisto-sleuth analyses - which provides increased sensitivity [17] - a total of 40 genes were found differentially expressed (Fig. 3B). The edgeR analysis identified 28 differentially expressed genes (16 upregulated and 12 downregulated), with at least a 1.25 fold change (FDR ≤ 0.05). Using kallisto gene counts and sleuth for differential expression analysis, 14 differentially expressed genes (8 upregulated and 6 downregulated) were identified with a 0.5 bias estimator value (FDR ≤ 0.05). Two genes DDAH1 and MELTF were found upregulated in both the edgeR and kallisto-sleuth analyses. Among a set of 10 upregulated genes that were partially randomly selected for RTqPCR validation, 8 genes (80%) were confirmed to be upregulated: DDAH1, ANGPTL4, ADAM19, CDKN1C, ZC3H18, GXYLT1, CUTA, and H3F3C. Conversely, of a selection of 7 downregulated genes only two genes (29%) were validated by RT-qPCR: CDH1 and GSTA4 (Fig. 3C). This could suggest a predominantly inhibitory role of the cytoplasmic HOTAIRM1 spliced isoforms (HM1-3 and HM1-2-3) on expression of a limited number of specific genes in CAKI-1 cells.

A Metascape enrichment analysis of the differentially expressed genes (DEGs) was performed to identify molecular pathways altered in the knockdown cells (http://www.metascape.org). This suggested a possible enrichment in genes related to the response to hypoxia (p=0.0014 for all 40 DEGs, or p=0.0032 for selectively the 23 upregulated genes). Further analysis of the specific set of upregulated genes using the Enrichr comprehensive database analysis tool (http://amp.pharm.mssm.edu/Enrichr) confirmed a significant enrichment in hypoxia upregulated genes (p=2.3E-5, adjusted p-value = 0.011; disease perturbations from GEO-up GSE4483 dataset; *ANGPTL4*, *SLC2A3*, *HLA-C*, *RPL7*, *NEAT1*). Consistent with a possible connection to hypoxia, Enrichr also retrieved ChIP-seq data from the ChEA 2016 database identifying HIF1 $\alpha$  target genes (p=0.005; *ANGPTL4*, *SLC2A3*, *STC2*).

To investigate the functions of the spliced *HM1-3* isoform we focused on *DDAH1* and *ANGPTL4*, two genes that were most deregulated in knockdown cells and are linked to hypoxia and angiogenesis pathways. We confirmed that the upregulation of both *ANGPTL4* and *DDAH1* mRNAs in *HOTAIRM1* knockdown CAKI-1 cells could be partially rescued by overexpression of the *HM1-3* isoform (Fig. 3D; Supplemental Fig. 6). These results supported the notion that the spliced *HM1-3* isoform contributes (at least in part) to the reduced steady state levels of the *DDAH1* and *ANGPTL4* mRNAs in these cells. Interestingly, this regulation is probably at the transcriptional level for *ANGPTL4*, since knockdown of *HM1-3* and *HM1-2-3* (with either siRNA #2 or #3) also increased the levels of the *ANGPTL4* pre-mRNA (Fig. 3E, see also below). In contrast, *DDAH1* pre-mRNA expression was unaffected suggesting a different post-transcriptional regulation of *DDAH1* 

mRNA levels (Supplemental Fig. 6). Consistent with these results and the above observation that *HM1-3* is the predominant isoform down-regulated in most ccRCC tumors, *ANGPTL4* was found significantly upregulated in the vast majority of TCGA ccRCC samples relative to their respective normal adjacent tissues (Fig. 3F, Supplemental Fig. 4B). In contrast, *DDAH1* mRNA was consistently downregulated in these ccRCC tumor samples (data not shown).

Since HOTAIRM1 expression was associated with a non-transformed or differentiated cellular state, we further analyzed the gene regulatory functions of HOTAIRM1 during neural and kidney lineage differentiation. Mouse Hotairm1 transcripts, which are highly expressed during RA-induced neural differentiation of ES cells (Supplemental Fig. 5), were knocked down during RA treatment in an shRNA-inducible mouse ES cell line (Supplemental Fig. 7A). As expected, this selectively inhibited expression of the most anterior Hoxa genes (Hoxa1-5), although Hoxa1 was only marginally affected and only after 96 h of induction with RA. Notably, Hotairm1 knockdown increased the expression of Angptl4 and reduced Ddah1 mRNA levels, concomitant with a modest induction of the pluripotency gene Sox2 (Supplemental Fig. 7B). Alternatively, mouse ES cells were differentiated into early renal lineages using a stepwise protocol that mimics in vivo development up to the nephrogenic intermediate mesoderm and early metanephric mesenchyme and ureteric bud stages, as previously described [40]. The progressive differentiation was verified by the expression of lineage stage-specific gene markers (Supplemental Fig. 8), Evaluation of the three main Hotairm1 isoforms showed a progressive increase in expression and a peak expression at the end of the induction process at day 8 (Fig. 3G). Knockdown of Hotairm1 in these renal progenitor cells showed slight reductions in OSR1 and GDNF expression (data not shown) and a large reduction in PAX2 expression (Fig. 3H). We did not observe significant changes in the expression of the other kidney lineage differentiation markers analyzed here. However, as seen above with CAKI-1 cells and ES-derived neural lineage cells, Hotairm1 knockdown also induced Angptl4 expression in these renal progenitor

Altogether, these results suggested a role of HOTAIRM1 during neural and renal lineage differentiation and in regulation of hypoxia signaling, including a possible indirect transcriptional regulation of ANGPTL4 by the cytoplasmic HM1-3 spliced isoform.

3.4. HOTAIRM1 is downregulated by hypoxia-mimetic stress and inhibits  $HIF1\alpha$  protein expression in normoxic cells

To explore the possible connection of *HOTAIRM1* with the hypoxia pathway, we exposed CAKI-1 cells to 100 µM cobalt chloride, a hypoxia-mimetic agent that inhibits prolyl hydroxylases and thereby

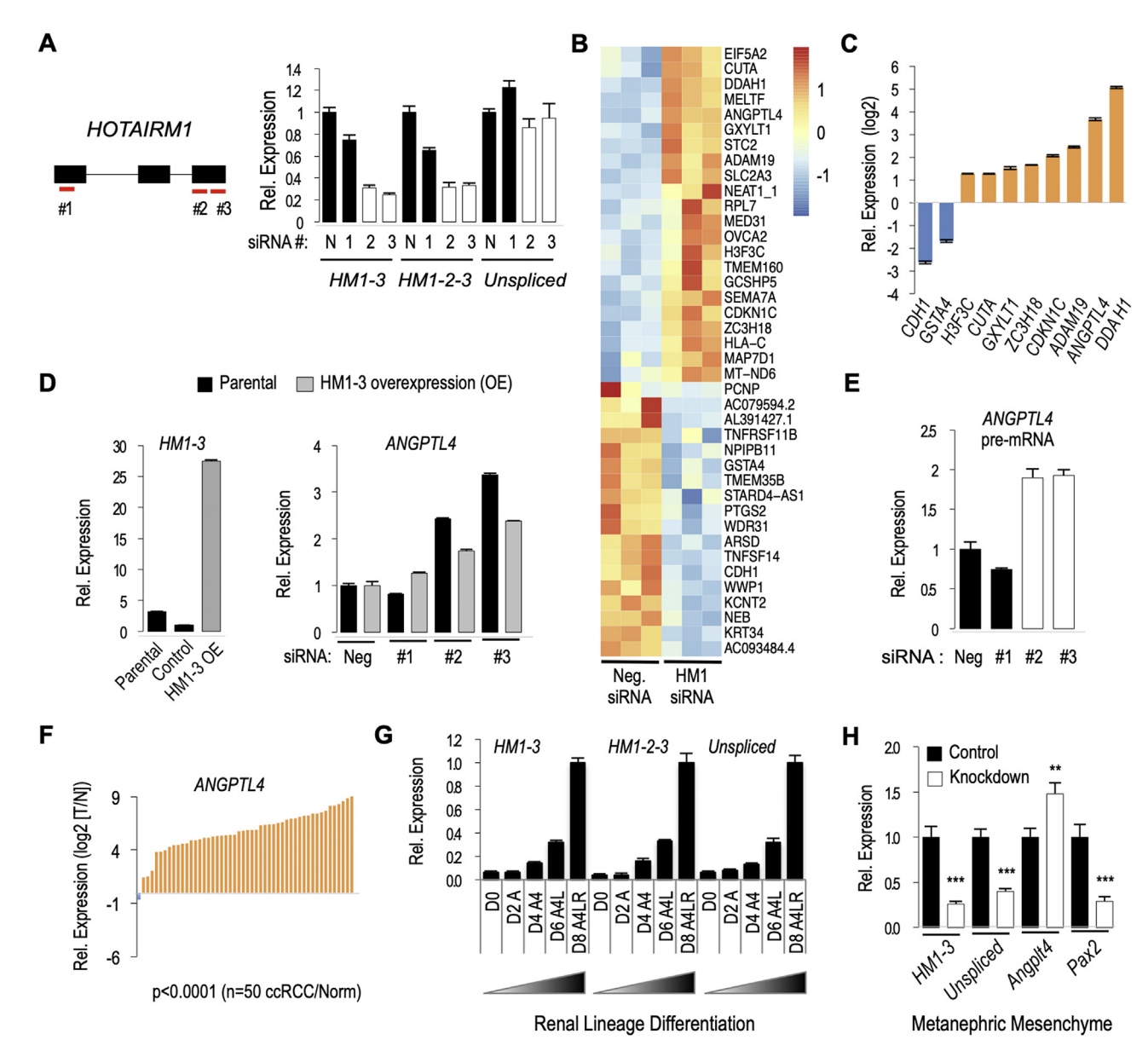


Fig. 3. Analysis of HOTAIRM1-dependent genes in human renal CAKI-1 cells and in differentiating mouse kidney progenitor cells identifies ANGPTL4 as a transcriptional target. A. HOTAIRM1 siRNAs (#2 and #3) selectively reduce the levels of the spliced isoforms (HM1-3 and HM1-2-3) in CAKI-1 cells. Expression relative to control (N) was analyzed by RT-qPCR. B. Knockdown of HOTAIRM1 spliced isoforms with siRNA#2 identifies 40 deregulated genes (DEGs) by combining edgeR (fold change > 1.25 and FDR < 0.05) and sleuth analyses ( $\beta$  > 0.5 and FDR < 0.05). C. Validation by qPCR of 10 DEGs in CAKI-1 cells. Shown is log2 fold change expression between control siRNA (N) and specific siRNA (#2) treated cells. D. Overexpression of ectopic HM1-3 inhibits ANGPTL4 induction upon knockdown of HOTAIRM1 in CAKI-1 cells. E. RT-qPCR analysis of ANGPTL4 pre-mRNA upon HOTAIRM1 knockdown. F. ANGPTL4 expression (log2 TPM tumor/normal ratios) in 50 ccRCC matched pair TCGA samples. Statistical significance was determined using the Wilcoxon signed rank test for the paired samples. G. Mouse Hotairm1 isoform expression by RT-qPCR during mES cell differentiation into kidney progenitor cells. D = day, A = Activin-A, 4 = BMP-4, L = LiCl, R = Retionic acid. H. RT-qPCR analysis of Angpl4 and Pax2 expression upon Hotairm1 knockdown in kidney progenitor cells. Two-tailed Student's t-test was used to determine statistical significance. Error bars represent SEM of technical replicates for A,C,D,E and biological replicates for G and H (\*\*p < 0.005, \*\*\*p < 0.0005).

prevents VHL-mediated ubiqutination and proteasomal degradation of HIF1 $\alpha$ . As anticipated, a time course analysis of cells treated with cobalt chloride showed a gradual induction of the HIF1 $\alpha$  protein (despite slight downregulation of *HIF1A* mRNA) and concomitant induction of the HIF1 $\alpha$  direct target gene *ANGPTL4*, peaking at approximately 4 h of treatment (Fig. 4A). In contrast, the *DDAH1* mRNA was not induced but seemed to decline during the 4–8 h treatment period. Interestingly, the levels of all *HOTAIRM1* transcripts remained relatively constant during the first 2 h of cobalt chloride treatment, and then rapidly decreased at 4 h and later time points (Fig. 4A). Thus, *HOTAIRM1* expression inversely correlates with both HIF1 $\alpha$  protein levels and expression of the *ANGPTL4* gene during cobalt chloride treatment. This suggested a

possible antagonist regulation between HOTAIRM1 and  $HIF1\alpha$  and the possibility that HOTAIRM1 negatively regulates  $HIF1\alpha$  expression under normoxic conditions. To test this, HOTAIRM1 spliced transcripts were knocked down in normoxic CAKI-1 cells (with siRNA #2 or #3). This resulted in stimulation of ANGPTL4, as expected, but interestingly also induced  $HIF1\alpha$  protein levels (Fig. 4B, top panel). Since HIF1A mRNA levels were not affected (Fig. 4B, bottom panel) this implies a negative posttranscriptional regulation of  $HIF1\alpha$  by the HOTAIRM1 spliced isoforms. Note also that the knockdown of HOTAIRM1 transcripts did not affect VHL protein expression (Fig. 4B).

To determine whether the negative regulation of *ANGPTL4* by the *HOTAIRM1* spliced isoforms involved suppression of the HIF1 pathway

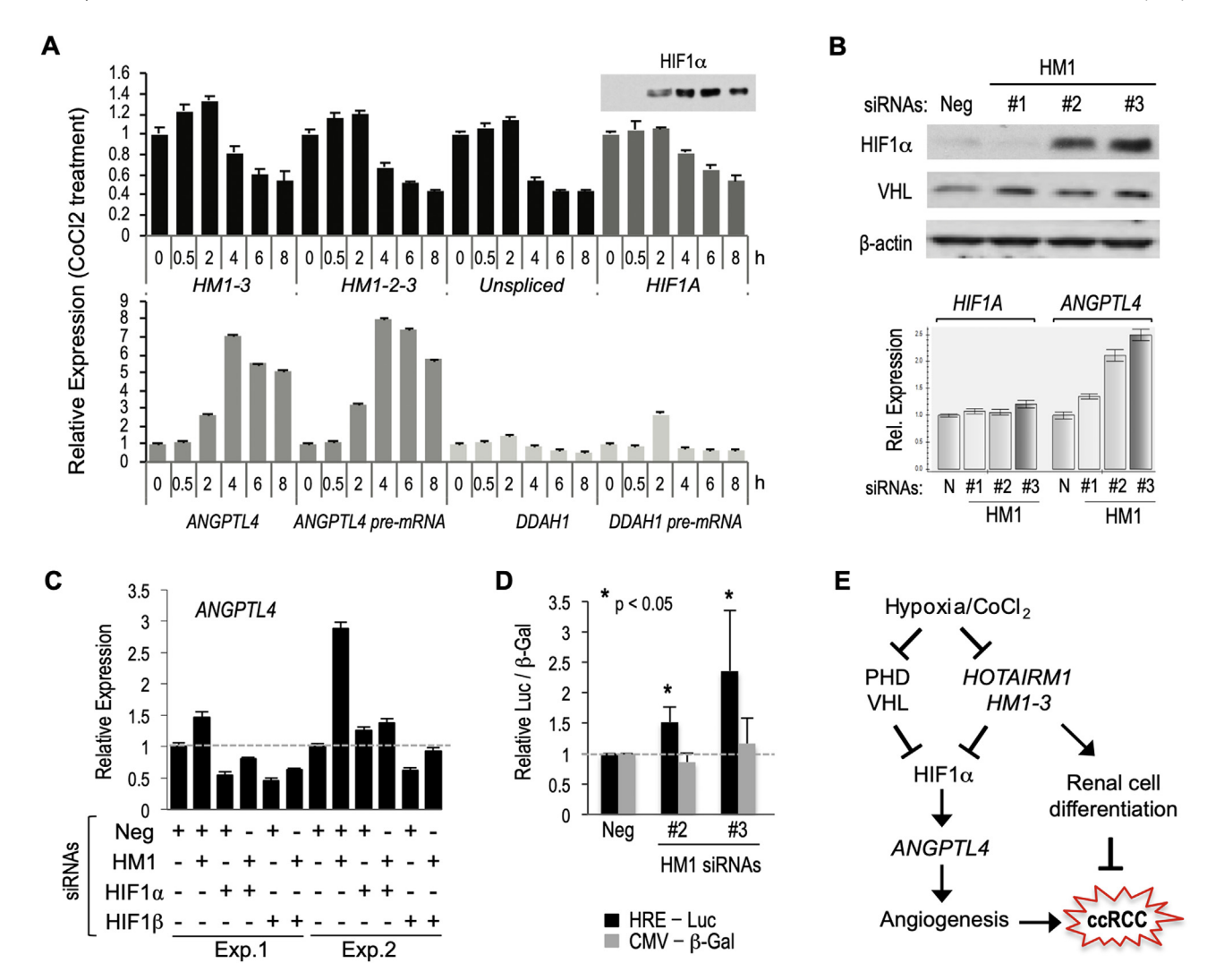


Fig. 4. Hypoxia-mimetic stress agent CoCl<sub>2</sub> downregulates HOTAIRM1 and HOTAIRM1 downregulation increases HIF1 $\alpha$  protein levels and HIF1 activity in normoxic renal cells. A. Gene expression analysis by RT-qPCR in CAKI-1 cells exposed to 100 μM cobalt chloride for the indicated times (0–8 h). HIF1A protein (HIF1 $\alpha$ ) levels were also analyzed by Western blot (inset above HIF1A). B. Western blot analysis of HIF1 $\alpha$  and VHL proteins in cells treated with the indicated siRNAs (top) and corresponding RT-qPCR analysis of HIF1A and ANGPTL4 expression (bottom). C. RT-qPCR analysis of ANGPTL4 expression in CAKI-1 cells treated with the indicated siRNAs against HOTAIRM1 (HM1) or HIF1 complex components (HIF1 $\alpha$  or HIF1 $\beta$ ). D. Knockdown of HM1 in normoxic CAKI-1 cells increases hypoxia response element-dependent transcription of a luciferase reporter gene (HRE-Luc) but does not affect expression of the co-transfected CMV- $\beta$ -Galactosidase reporter (CMV- $\beta$ -Gal). E. Schematic model of possible role of HOTAIRM1 lncRNA HM1-3 in kidney cell differentiation and ccRCC. The model does not differentiate a role of HM1-3 within the prolyl-hydroxylase (PHD)/VHL pathway or in a parallel pathway.

under normoxia, cells were depleted of either  $HIF1\alpha$  or its obligatory dimerization/DNA-binding partner  $HIF1\beta$  with specific siRNAs. Under these conditions knockdown of HOTAIRM1 failed to induce ANGPTL4 (Fig. 4C), indicating a requirement for HIF1 signaling. To further verify that HOTAIRM1 regulates the HIF1 pathway, the activity of a luciferase reporter gene under the control of three hypoxia-responsive DNA elements (HRE-Luc) was analyzed in cells transfected with either the negative control siRNA or the two HOTAIRM1-specific siRNAs (#2 and #3). Consistent with the above results, HOTAIRM1 knockdown stimulated the HRE-Luc reporter gene but not a co-transfected CMV- $\beta$ -Gal reporter plasmid (Fig. 4D). Altogether these analyses show that HOTAIRM1 expression is downregulated by hypoxia-mimetic stress and that its cytoplasmic spliced isoforms inhibit transcription of the ANGPTLA gene via a posttranscriptional mechanism that prevents HIF1 $\alpha$  protein accumulation and HIF1 signaling in normoxic cells.

#### 4. Discussion

In the current study, we provide new insights into the functional

role(s) of the HOTAIRM1 lncRNAs in kidney biology. Our analyses identify a novel and pervasive downregulation of the spliced HM1-3 isoform in ccRCCs, not previously reported. We demonstrate that HM1-3 is the only HOTAIRM1 isoform downregulated in ccRCC and is the most abundant HOTAIRM1 transcript found in normal kidney tissue. Furthermore, we show that HM1-3 is largely localized to the cytoplasm in all renal and non-renal cell lines analyzed. HOTAIRM1 is downregulated by hypoxia-mimetic stress and knockdown of its cytoplasmic isoforms in normoxic CAKI-1 cells leads to increased HIF1 $\alpha$  protein levels and upregulation of hypoxia-responsive genes, including the angiogenic ANGPTL4 gene. Our results reveal for the first time that HOTAIRM1 transcripts are induced during early renal lineage differentiation in vitro and are required for expression of several differentiation markers suggesting a possible role of HOTAIRM1 in kidney tissue differentiation and maintenance. Altogether, our results suggest the possibility of pro-differentiation and tumor-suppressive roles of HM1-3 in the kidney via attenuation of HIF1 signaling, an oncogenic pathway that is recurrently engaged in the vast majority of ccRCC tumors (Fig. 4E).

Our findings support a new, and possibly conserved, role of HOTAIRM1 during differentiation of normal ES cells into early renal and neural cell lineages that extends beyond its previously reported involvement in RA-induced myeloid and neural differentiation of cancer cell lines. The expression profiles of HOTAIRM1 during differentiation of mouse ES cells into early renal lineages mirrored the expression profiles of WNT11, GDNF and CDH11. Additionally, HOTAIRM1 appeared to be necessary to maintain the kidney progenitor state, as knockdown of HOTAIRM1 reduced expression of the kidney lineage differentiation markers, OSR1, GDNF and PAX2. Since knockdown of mouse Hotairm1 did not exclusively or preferentially affect HM1-3, it remains unclear which of the different lncRNA isoforms is responsible for this regulation. However, we suspect that HM1-3 is likely to be a major contributor as it is the most abundant Hotairm1 isoform in these early renal lineage cells and in adult kidney tissue. Notably, Angptl4 was downregulated by Hotairm1 during both neural and renal differentiation of mouse ES cells similar to human CAKI-1 cells, indicating a conserved regulatory pathway.

Mechanistically, we provide evidence that expression of both  $HIF1\alpha$ and HIF1\beta, is required for the increased transcription of ANGPTL4 premRNA observed upon depletion of cytoplasmic HOTAIRM1 splice variants in CAKI-1 cells. However, it remains unclear at this stage how HOTAIRM1 cytoplasmic isoforms inhibit posttranscriptionally the accumulation of the HIF1a protein in normoxic cells (i.e., without altering  $HIF1\alpha$  mRNA levels). Future analyses will address this important question. The fact that the HIF1 pathway is recurrently activated in ccRCC via the frequent inactivation of the VHL tumor suppressor [6,7] raises the important questions of whether HM1-3 is a bona fide tumorsuppressive lncRNA and whether it helps maintain low levels of HIF1  $\alpha$ protein levels in normoxic cells by functioning either as an intrinsic component of the VHL pathway or in a separate/parallel pathway. We show that during hypoxia-mimetic stress all HOTARM1 transcripts are downregulated raising the possibility that HIF1α accumulation during hypoxia might inhibit transcription of the HOTAIRM1 locus. It will be important to further characterize this potential negative feedback loop between HOTAIRM1 and HIF1 and determine whether its deregulation impacts ccRCC development. Furthermore, the fact that only the HM1-3 spliced isoform but not the primary unspliced HOTAIRM1 transcript is downregulated in ccRCC may suggest a defective HO-TAIRM1 splicing mechanism in this major kidney cancer that is worth further investigating. Note that while it remains unclear whether the reduced HM1-3 levels drive or are merely a consequence of ccRCC development, the reduced ratio of spliced (HM1-3) versus unspliced HOTAIRM1 observed in the vast majority of ccRCC tumors may be a new molecular indicator of this specific kidney malignancy, which is similar to - and consistent with - the recent identification of ANGPTL4 expression as a diagnostic marker of specifically ccRCC [41].

In conclusion, this study reveals a new function of *HOTAIRM1* in the kidney that is associated with renal cell differentiation and the hypoxia pathway, and uncovers the pervasive downregulation of its major HM1-3 cytoplasmic spliced isoform in ccRCC tumors.

#### Declaration of competing interest

No conflict of interest.

#### Acknowledgements

The results reported here are in part based upon data generated by The Cancer Genome Atlas (TCGA) managed by the NCI and NHGRI of the National Institutes of Health (NIH). Information about TCGA can be found at <a href="http://cancergenome.nih.gov">http://cancergenome.nih.gov</a>. This work was supported by a grant from NIH (R01CA158540). A.T.K. was supported by a MARC U-STAR training grant from the NIH (T34GM062756).

#### Appendix A. Supplementary data

Supplementary data to this article can be found online at https://doi.org/10.1016/j.canlet.2019.12.022.

#### References

- United States Cancer Statistics, Incidence and Mortality Web-Based Report, (1999-2014).
- [2] W. Seitz, K.H. Karcher, W. Binder, Radiotherapy of metastatic renal cell carcinoma, Semin. Surg. Oncol. 4 (2) (1988) 100–102.
- [3] R.E. Ferguson, S.M. Jackson, A.J. Stanley, A.D. Joyce, P. Harnden, E.E. Morrison, P.M. Patel, R.M. Phillips, P.J. Selby, R.E. Banks, Intrinsic chemotherapy resistance to the tubulin-binding antimitotic agents in renal cell carcinoma, Int. J. Cancer 115 (1) (2005) 155–163.
- [4] Cancer Facts & Figures 2018.
- [5] W.M. Linehan, M.M. Walther, B. Zbar, The genetic basis of cancer of the kidney, J. Urol. 170 (6 Pt 1) (2003) 2163–2172.
- [6] J.R. Gnarra, K. Tory, Y. Weng, L. Schmidt, M.H. Wei, H. Li, F. Latif, S. Liu, F. Chen, F.M. Duh, et al., Mutations of the VHL tumour suppressor gene in renal carcinoma, Nat. Genet. 7 (1) (1994) 85–90.
- [7] N. Cancer Genome Atlas Research, Comprehensive molecular characterization of clear cell renal cell carcinoma, Nature 499 (7456) (2013) 43–49.
- [8] J.J. Blondeau, M. Deng, I. Syring, S. Schrodter, D. Schmidt, S. Perner, S.C. Muller, J. Ellinger, Identification of novel long non-coding RNAs in clear cell renal cell carcinoma, Clin. Epigenet. 7 (2015) 10.
- [9] G.G. Malouf, J. Zhang, Y. Yuan, E. Comperat, M. Roupret, O. Cussenot, Y. Chen, E.J. Thompson, N.M. Tannir, J.N. Weinstein, et al., Characterization of long noncoding RNA transcriptome in clear-cell renal cell carcinoma by next-generation deep sequencing, Mol. Oncol. 9 (1) (2015) 32–43.
- [10] Y.Y. Tseng, B.S. Moriarity, W. Gong, R. Akiyama, A. Tiwari, H. Kawakami, P. Ronning, B. Reuland, K. Guenther, T.C. Beadnell, et al., PVT1 dependence in cancer with MYC copy-number increase, Nature 512 (7512) (2014) 82–86.
- [11] S.W. Cho, J. Xu, R. Sun, M.R. Mumbach, A.C. Carter, Y.G. Chen, K.E. Yost, J. Kim, J. He, S.A. Nevins, et al., Promoter of lncRNA gene PVT1 is a tumor-suppressor DNA boundary element, Cell 173 (6) (2018) 1398–1412 e1322.
- [12] M.J. Hamilton, M.D. Young, S. Sauer, E. Martinez, The interplay of long non-coding RNAs and MYC in cancer, AIMS Biophys. 2 (4) (2015) 794–809.
- [13] J.D. Gordan, J.A. Bertout, C.J. Hu, J.A. Diehl, M.C. Simon, HIF-2alpha promotes hypoxic cell proliferation by enhancing c-myc transcriptional activity, Cancer Cell 11 (4) (2007) 335–347.
- [14] J.D. Gordan, P. Lal, V.R. Dondeti, R. Letrero, K.N. Parekh, C.E. Oquendo, R.A. Greenberg, K.T. Flaherty, W.K. Rathmell, B. Keith, et al., HIF-alpha effects on c-Myc distinguish two subtypes of sporadic VHL-deficient clear cell renal carcinoma, Cancer Cell 14 (6) (2008) 435–446.
- [15] S. Grampp, J.L. Platt, V. Lauer, R. Salama, F. Kranz, V.K. Neumann, S. Wach, C. Stohr, A. Hartmann, K.U. Eckardt, et al., Genetic variation at the 8q24.21 renal cancer susceptibility locus affects HIF binding to a MYC enhancer, Nat. Commun. 7 (2016) 13183.
- [16] X. Liu, Y. Hao, W. Yu, X. Yang, X. Luo, J. Zhao, J. Li, X. Hu, L. Li, Long non-coding RNA emergence during renal cell carcinoma tumorigenesis, Cell. Physiol. Biochem. 47 (2) (2018) 735–746.
- [17] M.J. Hamilton, T. Girke, E. Martinez, Global isoform-specific transcript alterations and deregulated networks in clear cell renal cell carcinoma, Oncotarget 9 (34) (2018) 23670–23680.
- [18] X. Zhang, Z. Lian, C. Padden, M.B. Gerstein, J. Rozowsky, M. Snyder, T.R. Gingeras, P. Kapranov, S.M. Weissman, P.E. Newburger, A myelopoiesis-associated regulatory intergenic noncoding RNA transcript within the human HOXA cluster, Blood 113 (11) (2009) 2526–2534.
- [19] X. Zhang, S.M. Weissman, P.E. Newburger, Long intergenic non-coding RNA HOTAIRM1 regulates cell cycle progression during myeloid maturation in NB4 human promyelocytic leukemia cells, RNA Biol. 11 (6) (2014) 777–787.
- [20] X.Q.D. Wang, J. Dostie, Reciprocal regulation of chromatin state and architecture by HOTAIRM1 contributes to temporal collinear HOXA gene activation, Nucleic Acids Res. 45 (3) (2017) 1091–1104.
- [21] L. Wan, J. Kong, J. Tang, Y. Wu, E. Xu, M. Lai, H. Zhang, HOTAIRM1 as a potential biomarker for diagnosis of colorectal cancer functions the role in the tumour suppressor, J. Cell Mol. Med. 20 (11) (2016) 2036–2044.
- [22] X. Zhang, S. Sun, J.K. Pu, A.C. Tsang, D. Lee, V.O. Man, W.M. Lui, S.T. Wong, G.K. Leung, Long non-coding RNA expression profiles predict clinical phenotypes in glioma, Neurobiol. Dis. 48 (1) (2012) 1–8.
- [23] Y. Zhou, B. Gong, Z.L. Jiang, S. Zhong, X.C. Liu, K. Dong, H.S. Wu, H.J. Yang, S.K. Zhu, Microarray expression profile analysis of long non-coding RNAs in pancreatic ductal adenocarcinoma, Int. J. Oncol. 48 (2) (2016) 670–680.
- [24] M. Diaz-Beya, S. Brunet, J. Nomdedeu, M. Pratcorona, A. Cordeiro, D. Gallardo, L. Escoda, M. Tormo, I. Heras, J.M. Ribera, et al., The lincRNA HOTAIRM1, located in the HOXA genomic region, is expressed in acute myeloid leukemia, impacts prognosis in patients in the intermediate-risk cytogenetic category, and is associated with a distinctive microRNA signature, Oncotarget 6 (31) (2015) 31613–31627.
- [25] Z.H. Chen, W.T. Wang, W. Huang, K. Fang, Y.M. Sun, S.R. Liu, X.Q. Luo, Y.Q. Chen, The lncRNA HOTAIRM1 regulates the degradation of PML-RARA oncoprotein and myeloid cell differentiation by enhancing the autophagy pathway, Cell Death Differ. 24 (2) (2017) 212–224.

[26] L.E. Dow, P.K. Premsrirut, J. Zuber, C. Fellmann, K. McJunkin, C. Miething, Y. Park, R.A. Dickins, G.J. Hannon, S.W. Lowe, A pipeline for the generation of shRNA transgenic mice, Nat. Protoc. 7 (2) (2012) 374–393.

- [27] S. Dupasquier, A.S. Delmarcelle, E. Marbaix, J.P. Cosyns, P.J. Courtoy, C.E. Pierreux, Validation of housekeeping gene and impact on normalized gene expression in clear cell renal cell carcinoma: critical reassessment of YBX3/ZONAB/ CSDA expression, BMC Mol. Biol. 15 (2014) 9.
- [28] M. Jung, A. Ramankulov, J. Roigas, M. Johannsen, M. Ringsdorf, G. Kristiansen, K. Jung, In search of suitable reference genes for gene expression studies of human renal cell carcinoma by real-time PCR, BMC Mol. Biol. 8 (2007) 47.
- [29] N.L. Bray, H. Pimentel, P. Melsted, L. Pachter, Near-optimal probabilistic RNA-seq quantification, Nat. Biotechnol. 34 (5) (2016) 525–527.
- [30] C. Trapnell, A. Roberts, L. Goff, G. Pertea, D. Kim, D.R. Kelley, H. Pimentel, S.L. Salzberg, J.L. Rinn, L. Pachter, Differential gene and transcript expression analysis of RNA-seq experiments with TopHat and Cufflinks, Nat. Protoc. 7 (3) (2012) 562–578.
- [31] H. Pimentel, N.L. Bray, S. Puente, P. Melsted, L. Pachter, Differential analysis of RNA-seq incorporating quantification uncertainty, Nat. Methods 14 (7) (2017) 687–690.
- [32] D. Kim, B. Langmead, S.L. Salzberg, HISAT: a fast spliced aligner with low memory requirements, Nat. Methods 12 (4) (2015) 357–360.
- [33] M. Lawrence, W. Huber, H. Pages, P. Aboyoun, M. Carlson, R. Gentleman, M.T. Morgan, V.J. Carey, Software for computing and annotating genomic ranges, PLoS Comput. Biol. 9 (8) (2013) e1003118.

- [34] M.D. Robinson, D.J. McCarthy, G.K. Smyth, edgeR: a Bioconductor package for differential expression analysis of digital gene expression data, Bioinformatics 26 (1) (2010) 139–140.
- [35] D.J. McCarthy, Y. Chen, G.K. Smyth, Differential expression analysis of multifactor RNA-Seq experiments with respect to biological variation, Nucleic Acids Res. 40 (10) (2012) 4288–4297.
- [36] T.W.H. Backman, T. Girke, systemPipeR: NGS workflow and report generation environment, BMC Bioinf. 17 (2016) 388.
- [37] M.I. Love, W. Huber, S. Anders, Moderated estimation of fold change and dispersion for RNA-seq data with DESeq2, Genome Biol. 15 (12) (2014) 550.
- [38] M.D. Wilkerson, D.N. Hayes, ConsensusClusterPlus: a class discovery tool with confidence assessments and item tracking, Bioinformatics 26 (12) (2010) 1572–1573.
- [39] P. Novak, T. Jensen, M.M. Oshiro, R.J. Wozniak, M. Nouzova, G.S. Watts, W.T. Klimecki, C. Kim, B.W. Futscher, Epigenetic inactivation of the HOXA gene cluster in breast cancer, Cancer Res. 66 (22) (2006) 10664–10670.
- [40] M. Nishikawa, N. Yanagawa, N. Kojima, S. Yuri, P.V. Hauser, O.D. Jo, N. Yanagawa, Stepwise renal lineage differentiation of mouse embryonic stem cells tracing in vivo development, Biochem. Biophys. Res. Commun. 417 (2) (2012) 897–902.
- [41] J. Verine, J. Lehmann-Che, H. Soliman, J.P. Feugeas, J.S. Vidal, P. Mongiat-Artus, S. Belhadj, J. Philippe, M. Lesage, E. Wittmer, et al., Determination of angptl4 mRNA as a diagnostic marker of primary and metastatic clear cell renal-cell carcinoma, PLoS One 5 (4) (2010) e10421.

# **Supplemental Information**

# HOTAIRM1 IncRNA is downregulated in clear cell renal cell carcinoma and inhibits the hypoxia pathway

Michael J. Hamilton<sup>a</sup>, Matthew Young<sup>a</sup>, Kay Jang<sup>a</sup>, Silvia Sauer<sup>a</sup>, Vanessa E. Neang<sup>a</sup>, Alexia T. King<sup>a</sup>, Thomas Girke<sup>b</sup> and Ernest Martinez<sup>a,\*</sup>

# 1. Supplemental Materials and Methods

## Rapid Amplification of cDNA Ends (RACE)

RACE experiments were performed with RNA extracted from D3 mouse ES cells induced with 1  $\mu$ M RA for 24 hours. Cells were trypsinized and 1 x 10<sup>6</sup> cells were used for RNA extraction and RACE analyses using the SMARTer RACE 5'/3' kit (Clontech-TAKARA) according to manufacturer's instructions and by using RACE primers within introns. IGV, FinchTV and BLAST were used to design RACE primers and analyze and align sequencing results to the mouse genome. RACE sequences of *Hotairm1* 5' and 3' ends are shown in Supplemental Figure 9 (below).

### Absolute quantification of transcripts by qPCR

Standard qPCR curves were created by plotting Cq vs. known template cDNA amounts (ng) with a minimum of 5 serially diluted samples. The amount of initial product in a test qPCR reaction was calculated from the standard curve and converted into transcript amount/copy per cell based on the known (predetermined) total RNA per cell for each cell type analyzed and assuming 100% efficiency in conversion of RNA into cDNA.

#### Primers used for qPCR analyses

Primers for specific *HOTAIRM1* spliced isoforms were set on unique exon junctions (\*asterisks in primer sequences below). The primers designed to detect the unspliced isoforms were set within the introns. The PCR specificity (single product via melting curve and/or gel analysis) and efficiency (>90%) were verified with the selected primer pairs listed below (in a 5'-3' direction).

#### Mouse:

Hotairm1 E1-3	Fwd (ex1-3 junction*) GGCAAGAG*GTCTGTTTTCC			
	Rev (exon 3)	ACACCCCATTTTCAGTGTG		
Hotairm1 E1-2-3	Fwd (ex2-3 junction*	CTCACG*GTCTGTTTTTCCTG		
	Rev (exon 3)	ACACCCCATTTTCAGTGTG		
Hotairm1 Long	Fwd (intron2)	CTCCACTTGCTAACCTGACTTC		
	Rev (intron2)	AAGATTCTTGCCCTCACCAC		
Hotairm1 Short	Fwd (intron1)	AGCAGTAGGCTTATGCAGCTC		
	Rev (intron1)	GCTGCTCAAAAGACCAAAGG		
Hoxa1		CGCAGACCTTTGACTGGATG		
		CTGCTTGGTGGTGAAATTGG		
Hoxa2		TTCCAGCTCCAAAAGCTGAG		
		GCCACAAAGAATCCCTGG		

Hoxa3	ACACTGTTGACCAGCGAATG

AAAGACCAGAAGGGCAAAGG GTTCGAGAGCGCTTAGGTTC

Hoxa4

CCCTGGATGAAGAAGATCCAC

Hoxa5 **GTCAGGTAGCGGTTGAAGTG** 

CAAGCTGCACATTAGTCACG

Hoxa6 TCCTTCTCAAGCTCCAGTGTC

ACCGACCGGAAGTACACAAG

Hoxa7 TGGAATTCCTTCTCCAGTTCC

AAGCCAGTTTCCGCATCTAC

Hoxa9 CAGAAACTCCTTCTCCAGTTCC

ACAATGCCGAGAATGAGAGC

Hoxa<sub>10</sub> TCACTTGTCTGTCCGTGAGG

AAGAAACGCTGCCCTTACAC

Hoxa11 **GCAGACGCTTCTCTTTGTTG** 

CCAAATACCAGATCCGAGAGC

Hoxa13 TGGAACCAGATTGTGACCTG

AGAACTCGAACGGGAATACG

**TGCAGTACAACTCCATGACCAG** Sox2

**TGCGAGTAGGACATGCTGTAG** 

Oct3/4 AGCCGACAACAATGAGAACC

**GGCACTTCAGAAACATGGTC** 

Nanog CCAGTCCCAAACAAAAGCTC

**AACACAGTCCGCATCTTCTG** 

**Nestin** TTCCCTGATGATCCAACCTC

**AGTTCCCAGATTTGCCCTTC** 

**TGGTGTGAATACTCGGAGGTC** Setd5

TGGAGGTGGTTTAGGGATTG

Map2 AAACGTTCTTCCCTCCCAAG

CTCTGCGAATTGGTTCTGAC

Foxa2 GAGCAGCAACATCACCACAG

CGTAGGCCTTGAGGTCCAT

GACCGCGGCGGAACAAGATA Osr1

CACTGTGGGCAGGCCATTCA

Wnt11 GTGAAGTGGGGAGACAGGCT

CACGTCCTGGAGCTCTTGC

CGCTGACCAGTGACTCCAAT Gdnf

GCCGCTTGTTTATCTGGTGA ATGGGGCACTGTTGTCCTGT

Cdh11 CACCCCTTCATCATCATAG

CAGCCCACCTACTGGCTCTA

Brachury

GAGCCTGGGGTGATGGTA

Lim1 TGGACCGTTTCCTCTTGAAC

**TGTTCTCTTTGGCGACACTG** 

Pax2 **GTTCCCAGTGTCTCATCCAT** 

GGCGTTGGGTGGAAAGG

Wt1 CTTCCGAGGCATTCAGGATGT

CCGGCTATGCATCTGTAAGTGG

Tp53 GCAACTATGGCTTCCACCTG

TAGCTTATTGAGGGGAGGAGAG

Neat1 AATCCCTCTGACCAATGCAG

ACTTGGCCTCGAGAAGATTG

Ddah1 CAAAGGCATGTCTTGCTG

TTTCCATCTCCGAGTTGCTC

Angptl4 CTGTTTTGAGCCTTGAGCTG

ATGCACCCTTCAAAGACTCC

Actb ATCACAATGCCTGTGGTACG

CTAAGGCCAACCGTGAAAAG

Gapdh AATCTCCACTTTGCCACTGC

GTGAAGGTCGGTGTGAACG

Polr2a TGCGTACTAATTCCTGAAGTCTG

**CCTGACCCTAACCTATCCATTG** 

Human:

HOXA1

HM1-3 Fwd (exon1-3 junction\*) AAGATGAACTGGCGAGAG\*GTC

Rev (exon 3) TTTCAAACACCCACATTTCAACC

HM1-2-3 Fwd (exon 2) CATCGCGTTGTCATTGGAAC

Rev (exon 3-2 junction\*) TTCAGGCAAAACAGAC\*CGTGA

Unspliced Fwd (intron 2) GCAACAACCCAGTGACACAC

Rev (intron 2) TGCTTCGAAGTCAGGTTAGC

TTGACCCAGGTAGCCGTACT

TCTTCTCCAGCGCAGACTTT
MALAT1 AGGGACTGGAGCTGTTTATC

TGAACCAAAGCTGCACTGTG

RPL7 GCCATATATTGCATGGGGGTAC

TGCCATAACCACGCTTGTAG

ADAM19 AGCACTTGCCCCAAAGTTTC

AGCTCAAGGAAAGGGAGAAGC

H3F3C TGGTGGGTCTGTTGGAAGATAC

TGTCTTTGGGCATGATGGTG

MAP7D1 AAGGAGGCTGTGCAGAAAGAG

AGAAGCCATTCTTACTCCC

CUTA TGCAGCCTTTGTTACTTGCC

AATCTGAGGGATGAGGTTGACG

DDAH1 AGTGAATCTGCACAGAAGGC

ACAGTGAGTTTGTCGTAGCG

GXYLT1 TGGCTCATGCATGTAATCCC

ACTTTGTCACCTAGGCTGGTC

ZC3H18 GAGGACGATGATGGAGAAATCG

ACTGGGGTCCTTCACTTCAC

ANGPTL4 CGCCATTTTTGGTGAACTGC

TTGAAGTCCACTGAGCCATCG

CDKN1C ACGCACTAGCTCGGTTATTG

GCTACAGCTTGTGAGTGACC

PTGS2 ATGATTGCCCGACTCCCTTG

**TGGGGATCAGGGATGAACTTTC** 

ARSD CAGCATCTTCACGCAGCAC

**TGCGGGGTCGTGTAATGAAC** 

GSTA4 CAGTTGTACAAGTTGCAGGATGG

TCCCGTCAATTTCAACCATGGG

CDH1 AATGGGGCAATCGCTTCAAG

ACCACCAGCAACGTGATTTC

WDR31 TGGCTGCTTTGAACTCAGAC

TGGTGATCTCATGTTCATGTCC

TNFRSF11B ATTTGGAGTGCAAGCTG

AGGGTGCTTTAGATGACGTCTC

WWP1 CTGCCGATGACACTGTTAATGG

TACTGGAGTACCCGTGACAG

ANGPTL4 pre-mRNA ACAGCTGGCATTCATGGAAG

AGTGACCAGGAAGACGCTTTC

DDAH1 pre-mRNA AGGCCCTAACTGCTCTTCAAAG

TCTACCCTGTCAAATGCCATCC

HIF1A/α ACAGTAACCAACCTCAGTGTGG

ATGGGTGAGGAATGGGTTCAC

## siRNAs used in Hotairm1 knockdown experiments

Human HOTAIRM1:

HM1 siRNA #1 UCAAUGAAAGAUGAACUGGtt
HM1 siRNA #2 CUGGGAGAUUAAUCAACCAtt
HM1 siRNA #3 GGAGACUGGUAGCUUAUUAaa

Mouse *Hotairm1*:

e3-3.7 (exon 3) GGAACGTAGATGTTTGAAA I-4.8/E3#1 (exon 3) CCCAAGCCCATTTCTATTA

Generation of KH2 mouse ES cell lines expressing doxycycline-inducible shRNAs. The shRNA design, expression vector constructs and KH2 clonal cell line selection were as previously described (Dow et al., 2012). Co-transfection of the pCol-TGM (shRNA expression vector) and pCAGGS-FIpE recombinase vector into KH2 mES cells was performed using Lipofectamine 3000 according to manufacturer specifications. The shRNA names and target sequences used are as follows:

E3#1: CCCAAGCCCATTTCTATTA Luc1309: CGGCTGAAGAGCCTGATCA

To induce Hotairm1 knockdown during early RA-induced neural differentiation of KH2 cells 1  $\mu$ g/ml of doxycycline (Sigma) was added to the cell culture medium 24 hours

before the addition of RA and doxycyline was maintained in the culture medium during the RA treatment (2-3 days, as indicated) with medium change every day.

#### Microscopy

Fluorescence microscopy pictures of GFP-expressing mouse KH2 ES cells were taken on a Nikon TE2000U with incorporated camera at 150x magnification with NIS Elements Software as well as Phase Contrast images used as a positive control. Other phase contrast microscopy was performed with a Zeiss Axiovert 25 at 40x magnification and pictures were taken with an iPhone 7S.

#### Transient transfection, Luciferase and Beta-galactosidase assays

On day 1, CAKI-1 cells at ~70% confluency were transfected in 12-well plates with the siRNAs (100nM final) using Lipofectamine3000 per manufacturer's instructions. The medium was changed with complete growth medium12h later. On day 3 the cells were transfected with Lipofectamine3000 and the reporter plasmids: 3.6ug HRE-Luciferase (a gift from Navdeep Chandel; Addgene plasmid #26731; Emerling et al. 2008) and 3.6ug pCMV- $\beta$ -Galactosidase. On day 4 cell extracts were prepared and luciferase and  $\beta$ -galactosidase assays were performed as previously described (Zhang et al., 2014; Liu et al., 2003). Relative luciferase units were normalized to  $\beta$ -galactosidase activity and  $\beta$ -galactosidase activity was normalized to cellular protein. Results were the average and standard deviation of 4 independent experiments each performed in triplicates. Student's t-test p value<0.05 (one-tailed) was considered a significant increase in expression relative to cells transfected with the control (Neg) siRNA.

# 2. Supplemental References

Dow, L.E., Premsrirut, P.K., Zuber, J., Fellmann, C., McJunkin, K., Miething, C., Park, Y., Dickins, R.A., Hannon, G.J., and Lowe, S.W. (2012). A pipeline for the generation of shRNA transgenic mice. Nat Protoc *7*, 374-393.

Emerling, B.M., Weinberg, F., Liu, J.L., Mak, T.W., and Chandel, N.S. (2008). PTEN regulates p300-dependent hypoxia-inducible factor 1 transcriptional activity through Forkhead transcription factor 3a (FOXO3a). Proc Natl Acad Sci USA *105*, 2622-2627.

Zhang, N., Ichikawa, W., Faiola, F., Lo, S.Y., Liu, X., and Martinez, E. (2014). MYC interacts with the human STAGA coactivator complex via multivalent contacts with the GCN5 and TRRAP subunits. Biochimica et Biophysica Acta (BBA)-Gene Regulatory Mechanisms *1839*, 395-405.

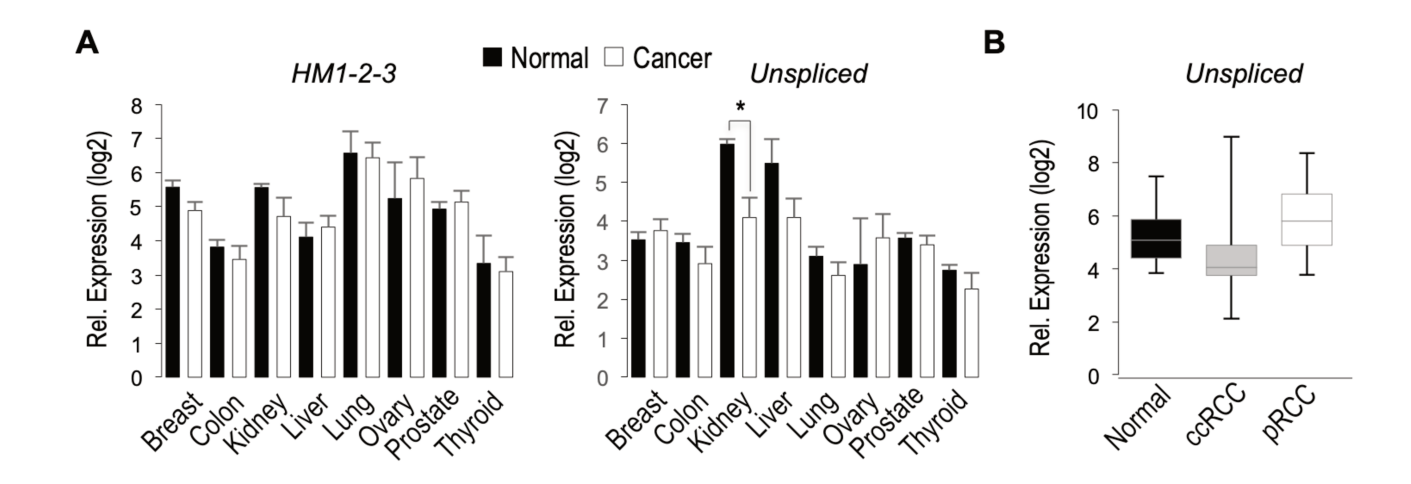
Liu, X., Tesfai, J., Evrard, Y.A., Dent, S.Y.R., and Martinez, E. (2003). c-Myc transformation domain recruits the human STAGA complex and requires TRRAP and GCN5 acetylase activity for transcription activation. J. Biol. Chem. *278*, 20405-20412.

# 3. Supplemental Tables

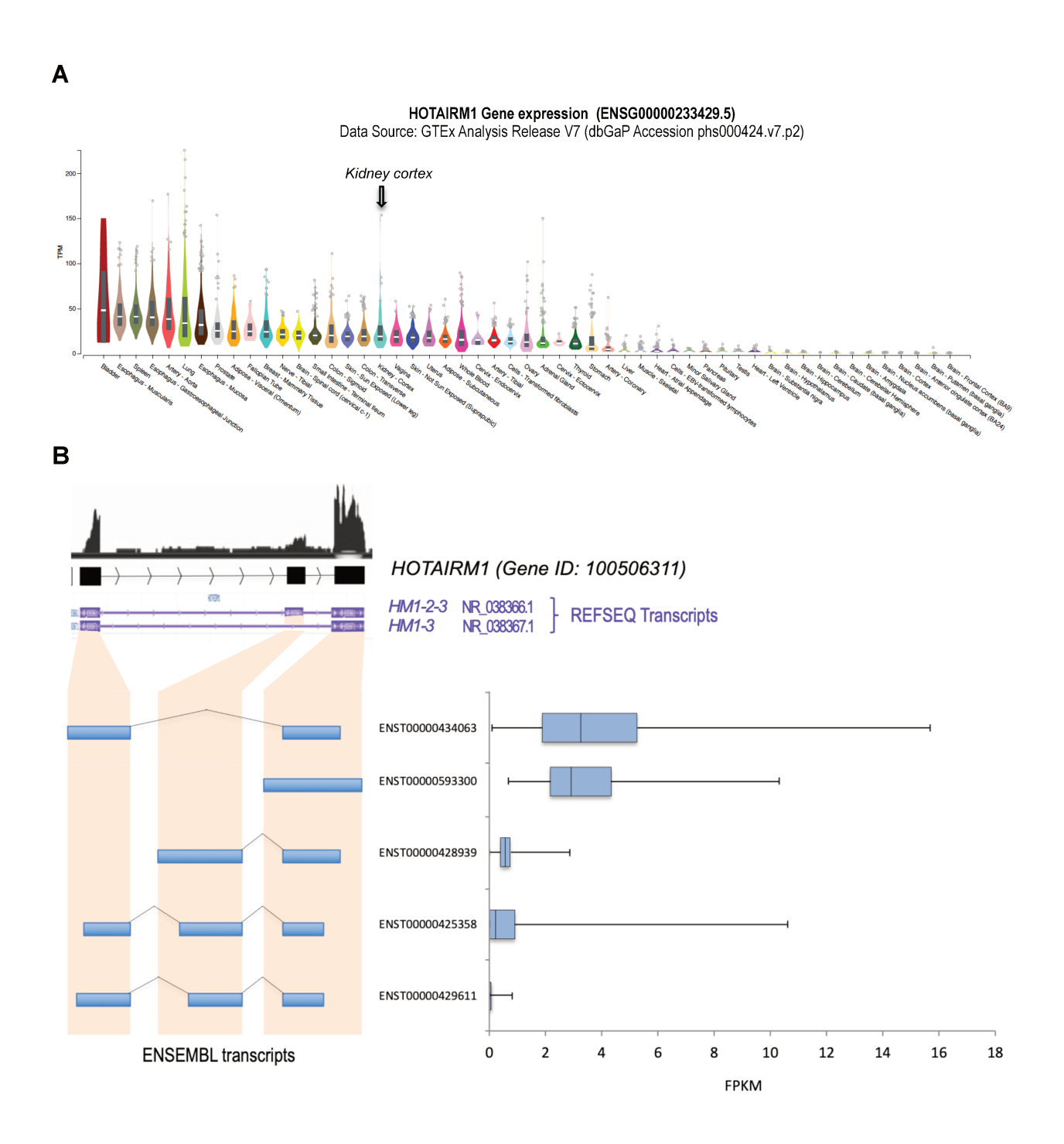
Table S1: Origene matched pair ccRCC tumor/normal RNA samples.

Match Pair #	Catalog Number	Case ID	Sample Classification
1	CR563036	CU0000000807	Tumor
	CR562944	CU0000000807	Normal
2	CR559247	CU0000006303	Tumor
	CR561460	CU0000006303	Normal
3	CR560088	CI0000010082	Tumor
	CR560086	CI0000010082	Normal
4	CR561100	CI0000000216	Tumor
	CR559748	CI0000000216	Normal
5	CR560856	CI0000005561	Tumor
	CR560857	CI0000005561	Normal
6	CR560960	CI0000005877	Tumor
	CR560957	CI0000005877	Normal
7	CR560907	CI0000006155	Tumor
	CR560906	CI0000006155	Normal
8	CR559302	CI0000006640	Tumor
	CR560658	CI0000006640	Normal
9	CR559596	CI0000009997	Tumor
	CR560141	CI0000009997	Normal
10	CR561841	CU0000011475	Tumor
	CR559696	CU0000011475	Normal
11	CR559768	CU0000012615	Tumor
	CR561775	CU0000012615	Normal
12	CR559682	CU0000012830	Tumor
	CR561813	CU0000012830	Normal

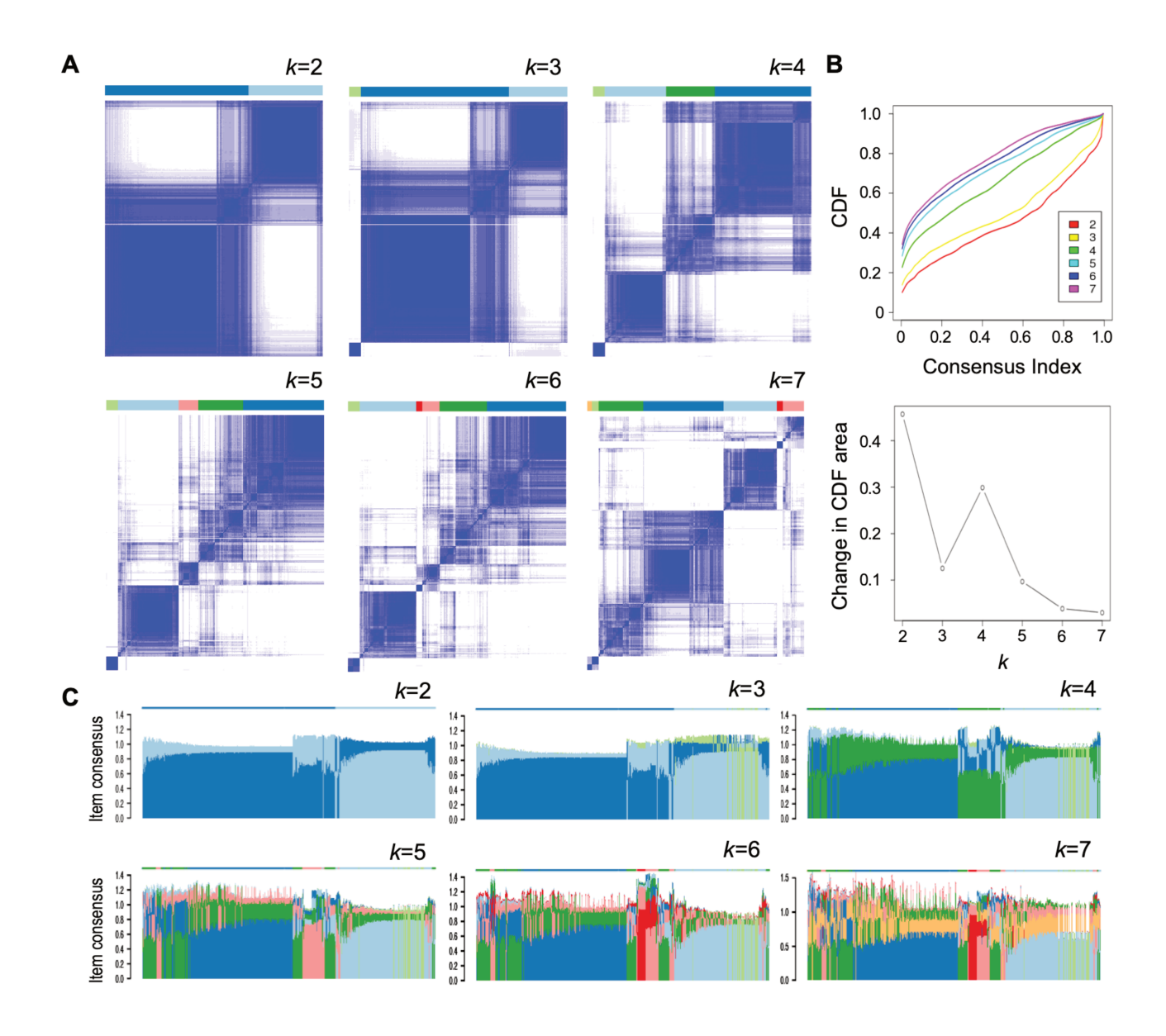
# 4. Supplemental Figures



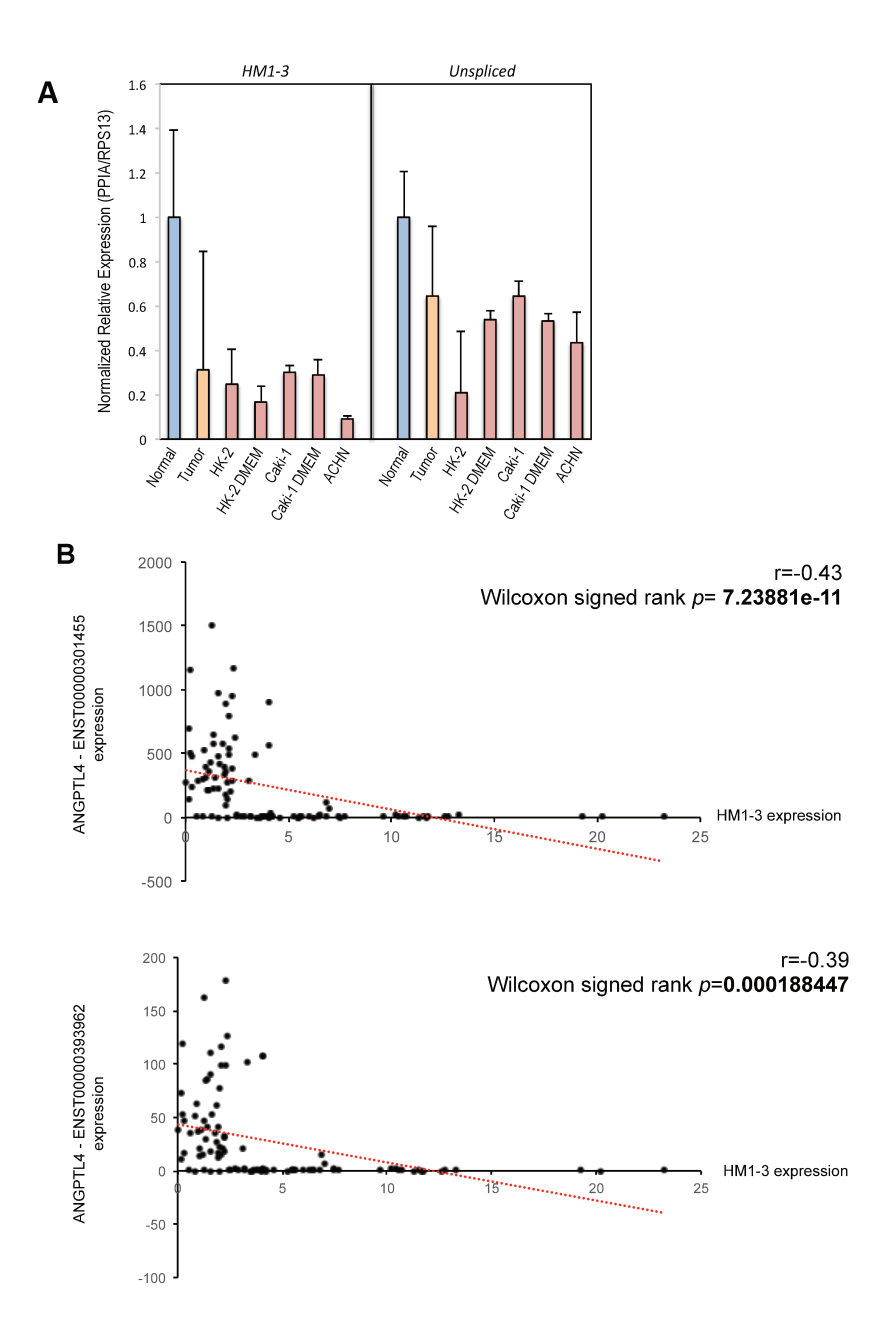
Supplemental Figure 1. Expression of *HOTAIRM1* unspliced transcript and spliced *HM1-2-3 isoform* in ccRCC. (A) Relative expression of *HM1-2-3* and *Unspliced* transcripts in eight human cancers relative to their respective normal tissue. *HM1-2-3* and *Unspliced* transcripts levels were analyzed by qPCR and normalized commercially to ACTB ( $\beta$ -actin). (B) Analysis of *Unspliced HOTAIRM1* expression by qPCR in normal tissues (n=9) versus ccRCC (n=21) and pRCC (n=10, papillary renal cell carcinoma) tumors was performed as in panel A. No significant differential expression of the *Unspliced* transcript was observed in ccRCC or pRCC. Statistical significance was determined by using two-tailed Student's t-test for all panels (\* p<0.05).



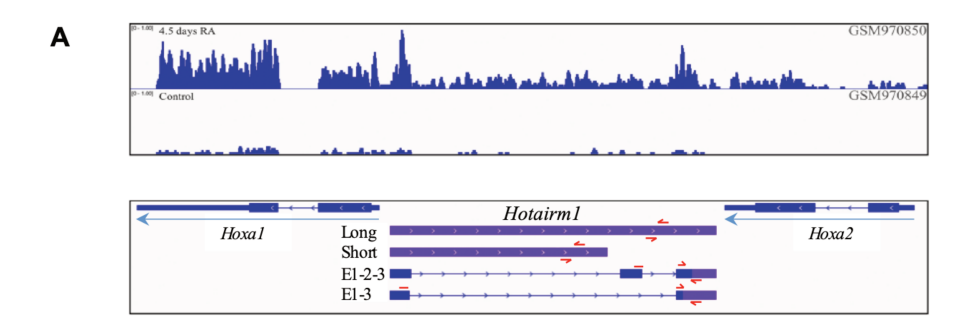
**Supplemental Figure 2.** *HM1-3* is the most abundant *HOTAIRM1* isoform expressed in normal kidney tissue. (A) *HOTAIRM1* gene expression (TPM) in different tissues was retrieved from the GTEx database. Kidney cortex is indicated with an arrow. (B) Quantitation of *HOTAIRM1* transcripts in 72 normal renal samples from the TCGA. Merged RNA-seq files from the 72 normal adjacent renal tissues of TCGA were aligned to the genome and to REFSEQ transcripts (top); annotated ENSEMBL transcripts were quantified (FPKM) using cufflinks (bottom).

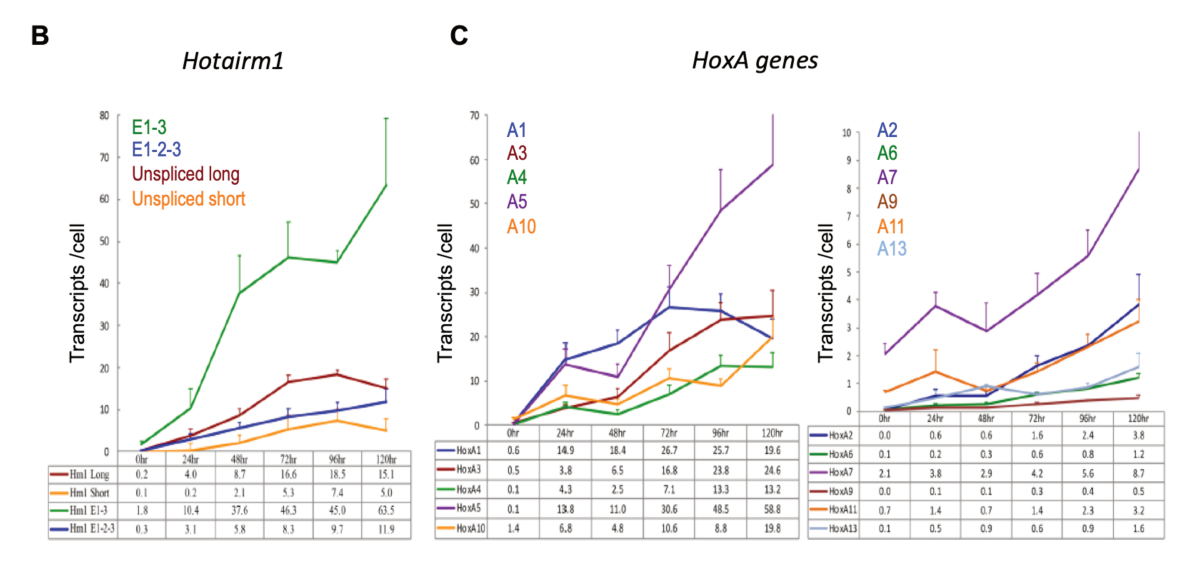


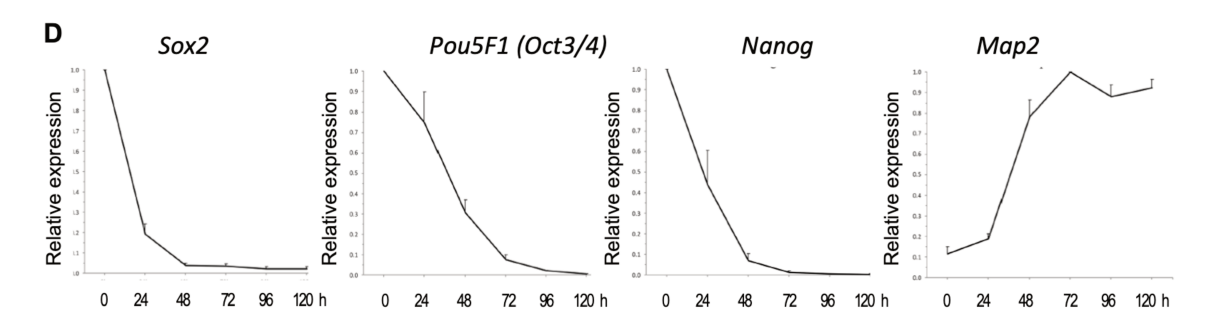
**Supplemental Figure 3. Four major ccRCC subtypes identified. (A)** Consensus matrices generated for k=2-7, using 1000 of the most variable genes. **(B)** Cumulative distribution functions (CDF) for each k of the consensus matrix (top). Greatest relative change in the area under the CDF curves observed from k=3 to k=4 (bottom). **(C)** Mean item consensus value for each cluster at a given k.



Supplemental Figure 4. (A) Expression of *HOTAIRM1* spliced isoform *HM1-3* is reduced in ccRCC tumors and renal cell lines. RT-qPCR analyses were performed with 1 ug of total RNA and normalized to the expression of *PPIA* and *RPS13*. Expression results are presented relative to normal kidney tissue, which was set to 1.0 (n=3 normal/tumor matched pairs). The cell lines were cultured *in vitro* in culture medium recommended by ATCC or in DMEM/10% FBS for ACHN and as indicated. (B) Expression of *HM1-3* and *ANGPTL4* mRNAs are inversely correlated in renal tissue. One hundred clinical samples from TCGA (50 ccRCCs and 50 normal adjacent tissues) were evaluated by plotting the fpkm values for *HM1-3* and for the two major *ANGPTL4* transcripts (top and bottom); the fpkm values were calculated with cufflinks.

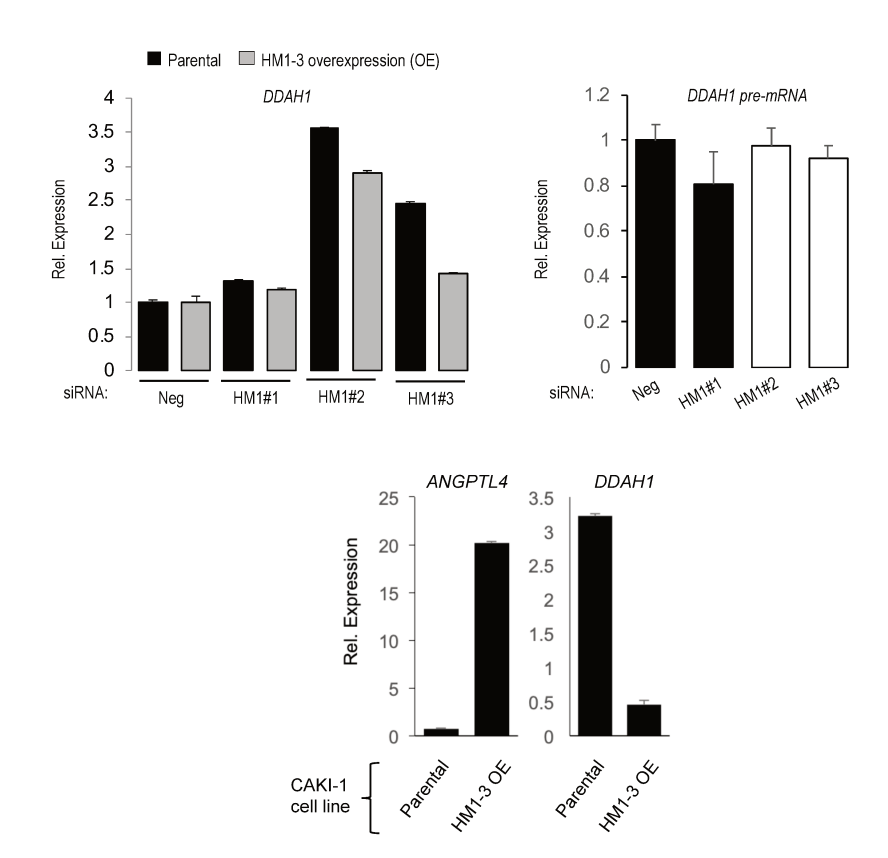




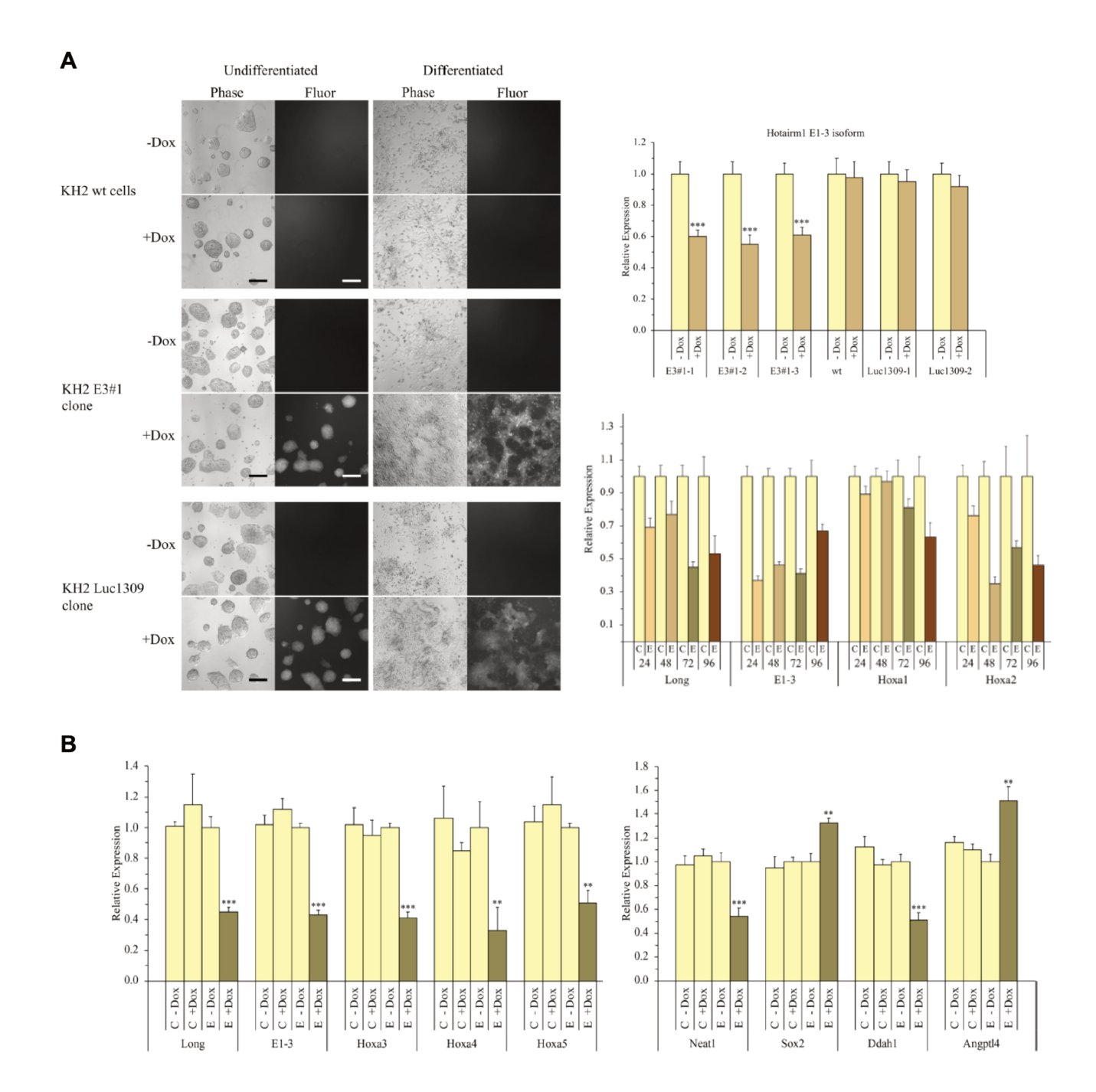


**Supplemental Figure 5. Characterization of Hotairm1 isoforms in mouse ES cells during early neural differentiation induced with RA. (A)** Top: RNA-seq track data available on Gene Expression Omnibus (GEO) of E14 mESCs treated with All-trans Retinoic Acid for 4.5 days. GEO accession numbers are shown to the right and treatment type is indicated on the left. Bottom: *Hotairm1* isoforms were aligned to the mouse mm9 genome. Unspliced transcripts were aligned based on the RACE results and spliced transcripts are from Ensembl annotations with the extended purple boxes at the 3' end of the spliced transcripts indicating the new 3'-ends based on our RACE results (see 5'-end and 3'-end RACE sequences in Supplemental Figure 10). Approximate locations of primers used for qPCR are indicated with red arrows. **(B) & (C)** Absolute quantification by RT-qPCR (transcripts/cell) showing induction of *Hotairm1* and *Hoxa* transcripts during the early differentiation of D3 mESCs (0-120h) continuously

treated with RA. **(D)** Relative expression by RT-qPCR showing expression of pluripotency and neural markers during early differentiation of D3 mESCs continuously treated with RA. Shown are pluripotency genes (*Sox2*, *Oct3/4*, *Nanog*) and a neurogenesis marker (*Map2*) during the first 120-hour period of differentiation. All results were derived from at least three biological replicates with error bars indicating standard error of the mean (SEM) and qPCR results were normalized to three housekeeping genes (*Gapdh*, *Polr2a*, and *Actb*).

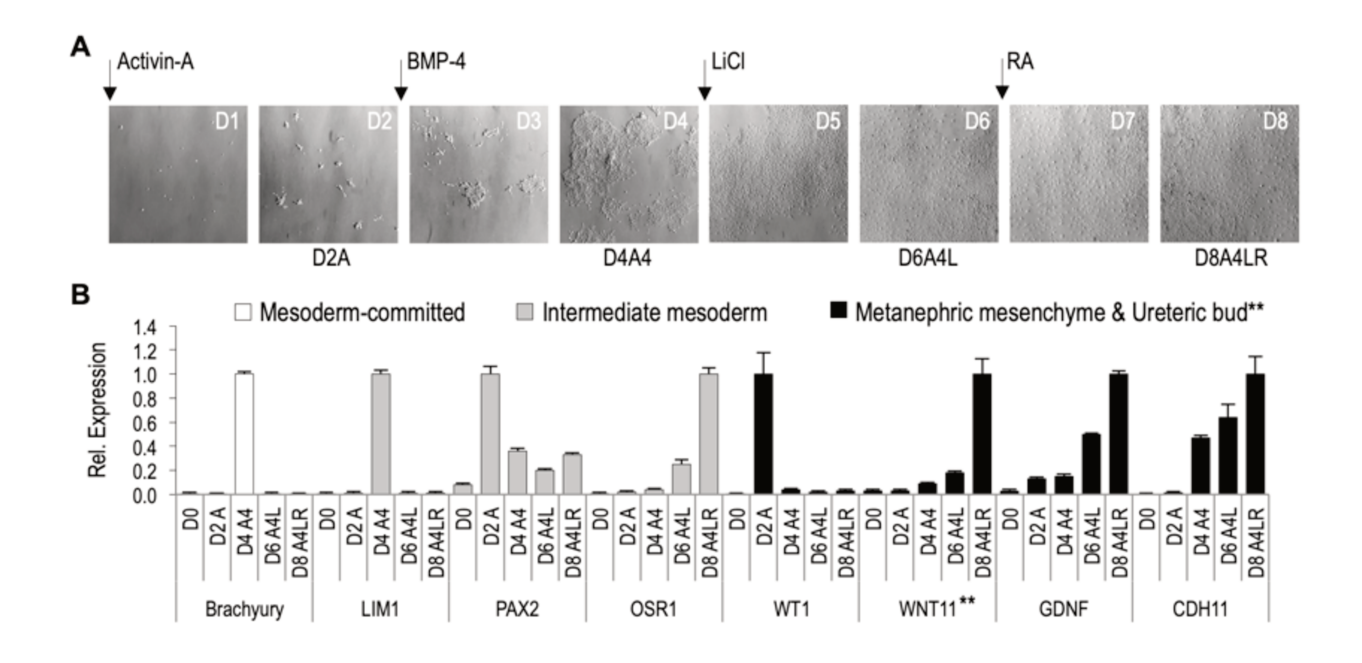


Supplemental Figure 6. *HM1-3* regulates *DDAH1* at the post-transcriptional level. RNAi-mediated knockdown of *HM1-3* in CAKI-1 cells increases the levels of *DDAH1* mRNA in normal CAKI-1 cells (parental) but less so in HM1-3 overexpressing cells (Top left) and does not affect synthesis of *DDAH1* pre-mRNA (Top right). The expression levels of *DDAH1* and *ANGPTL4* mRNAs in CAKI-1 parental and HM1-3 overexpressing (HM1-3 OE) cells are shown in the bottom panel. Expression analyses were performed by RT-qPCR.

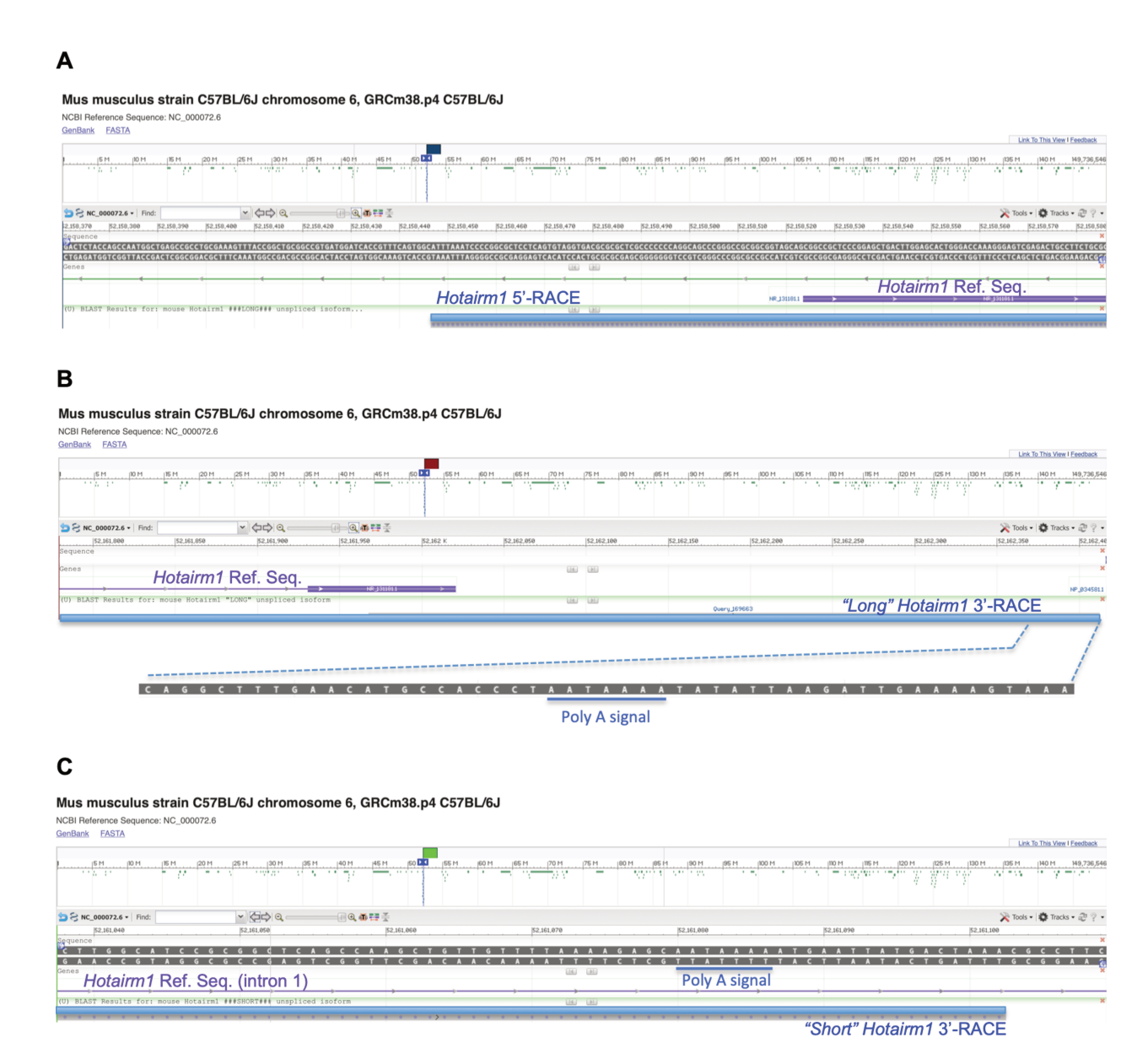


Supplemental Figure 7. Knockdown of *Hotairm1* during early RA-induced neural differentiation of KH2 mESCs induces expression of *Angptl4* and inhibits *Ddah1* and anterior *Hoxa* genes. (A) Left: Images of wild type (wt) KH2 mES cells and derivative cell lines engineered to express doxycycline (Dox)-inducible shRNAs against *Hotairm1* (E3#1-2) or against luciferase (Luc1309-1), as control. Upon treatment with Doxycycline cells express the shRNA and green fluorescent protein (GFP) as seen in the "Fluor" column. Scale bar is equivalent to 100  $\mu$ m. Cells were seeded on 0.1% gelatin coated cell-culture plates at a density of 1 x 10<sup>4</sup> cells/cm<sup>2</sup>. Cells were treated with or without 1  $\mu$ g/ml Doxycycline ("+ Dox" or "- Dox") for four days in the presence of LIF ("Undifferentiated" column) or without LIF plus 1  $\mu$ M RA ("Differentiated" column) for

three days with media changes every 24 hours. "Phase" indicates phase contrast microscopy images and "Fluor" indicates fluorescence microscopy images with an enhanced GFP (EGFP) filter. Pictures were taken on a Nikon TE2000U microscope with incorporated camera at 150x magnification using NIS Elements Software. The E3#1 shRNA targets exon 3 of Hotairm1 within the new sequences identified by the 3'-RACE results and Luc1309 shRNA targets Luciferase at nucleotide 1,309 (see sequences above in Supplemental Materials and Methods). (A) Right top panel: relative expression of the Hotairm1 E1-3 isoform in RA-treated Dox-inducible shRNA KH2 cell lines in the absence and presence of doxycycline (Dox). KH2 mESC wild type (wt) and different DOX-inducible shRNA clonal cell lines (E3#1-1, -2, and -3, and Luc1309-1, and -2) were seeded on 0.1% gelatin coated plates and treated with or without 1 µg/ml Doxycycline ("+ Dox" or "- Dox") for three days, and for the last two days in media also containing 1 μΜ RA (+ RA), with media changes every 24 hours. Relative Expression by RT-qPCR was performed using primers across exon 1-3 junction and within exon 3 (see sequences in Supplemental Materials and Methods above) which selectively detect the major Hotairm1 E1-3 isoform. Shown are the results of three biological replicates with error bars indicating standard error of the mean (SEM) and normalized to Gapdh, Polr2a, and Actb. Three asterisks (\*\*\*) indicate statistical significance (p< 0.001). (A) Right bottom panel: Doxycycline treatment induces knockdown of both the unspliced transcript and the E1-3 major spliced isoform and inhibits differentially expression of Hoxa1 and Hoxa2 during RA-induced differentiation of KH2 mES cells (clone E3#1-2; E). The Dox-inducible Luc shRNA KH2 cell line (Luc1309-1; C) served as a negative control. Cells were pre-treated with 1 µg/ml Doxycycline for 24 hours, then with 1 µM RA and 1µg/ml Doxycycline for the indicated times (up to 96 hours) with media changes every 24 hours. For each time point RT-qPCR was performed as above with specific primers for the indicated Hotairm1 and Hoxa transcripts and expression is shown relative to the control cell line (C). (B) Knockdown of Hotairm1 upregulates Angptl4 expression and downregulates Ddah1 and anterior Hoxa genes during RA-induced neural differentiation of mES cells. KH2 ES cell lines E3#1-2 denoted "E" and control Luc1309-1 denoted "C" were pre-treated with or without 1 µg/ml Doxycycline (+ Dox or – Dox) for 24 hours, then with 1 µM RA, plus or minus doxycycline, for 72 hours with media changes every 24 hours. Relative expression of the indicated genes/transcripts was analyzed by RTqPCR and normalized to Gapdh, Polr2a, and Actb, as above. The asterisks indicate statistical significance: \*\*\*p < 0.001, \*\*p < 0.01, and \*p < 0.05. Shown are the results of three biological replicates with error bars indicating standard error of the mean (SEM).



**Supplemental Figure 8. Differentiation of mouse ES cells into kidney progenitor cells. (A)** KH2 mES cells were sequentially exposed to activin A (Day 0, D0), BMP-4 (Day 2, D2), LiCL (Day 4, D4) and RA (Day 6, D6) to differentiate into kidney progenitor cells. A=activin A, 4=BMP-4, L=LiCL, R=RA. **(B)** Relative mRNA expression by RT-qPCR of mesoderm-commitment, intermediate mesoderm and metanephric mesenchyme markers during the differentiating time course. WNT11 is a marker specific of the ureteric bud (\*\*). Gene expression was normalized to *Gapdh*, *Polr2a*, and *Actb*. Error bars represent SEM for three biological replicates.



Supplemental Figure 9. Mouse *Hotairm1* transcripts 5' and 3' ends identified by RACE sequencing results in RA-treated mES cells. (A) Nucleotide sequence of the 5' end of *Hotairm1* relative to the annotated Reference Sequence in NCBI (shown in purple). (B) Sequence of the 3' end of the unspliced *Hotairm1* "Long" isoform and location of the polyadenylation signal (Poly A signal, underlined). (C) Sequence of the 3' end of the newly identified unspliced *Hotairm1* "Short" isoform with its Poly A signal (underlined).